

Defects in Superfluids, Superconductors and Membranes*

David R. Nelson

Lyman Laboratory of Physics, Harvard University, Cambridge, MA 02138

Abstract

An introduction to the defects which dominate the physics of superfluid He^4 films, of superconducting slabs and of crystalline and hexatic membranes is given. We first review point vortices in two-dimensional neutral superfluids and discuss the unusual screening which arises when the bosons are charged, as in superconducting films. Dislocation and disclination defects in crystalline membranes are discussed from a similar point of view. There is little or no screening in “monolayer” crystals, which are strongly constrained to lie in a flat two-dimensional plane. A strong nonlinear screening effect arises, however, in 2d membranes allowed to buckle into the third dimension. This screening drastically lowers dislocation and disclination energies, and forces crystalline membranes to melt at any finite temperature. We point out that buckled 5- and 7-fold disclinations in hexatic membranes have in general different logarithmically divergent energies. A similar asymmetry exists in the energies of 5- and 7-fold defects in *liquid* membranes. This difference determines the sign of the Gaussian bending rigidity, and has important consequences in membranes which can change their topology or with free boundary conditions.

* Lectures given at the NATO ASI on Fluctuating Geometries in Statistical Mechanics and Field Theory, Les Houches, Summer 1994.

I. INTRODUCTION

Phase transitions and spontaneous symmetry breakings abound in modern condensed matter physics. Of particular interest are the low energy excitations associated with *continuous* broken symmetries, like the broken translational and orientational invariance of a crystal, the broken rotational symmetry of ferromagnet or the broken gauge symmetry of superfluids and superconductors. By imposing a slow spatial variation of the continuous symmetry operation on the ground state, one generates an important class of modes which can be easily excited near $T = 0$. In ferromagnets for example, these Goldstone modes are called spin waves, or, in quantized form, “magnons.” In crystalline solids, the translational broken symmetry leads to new shear phonon modes. Unlike a nematic liquid crystal, the additional broken rotational symmetry of a solid does *not* lead to any extra low energy modes: Rotational modes are coupled to phonons in a way reminiscent of the Higgs mechanism and are thus rendered massive—see Ref. [8] below and references therein. In superfluid helium, the broken symmetry selects a particular phase for the condensate order parameter, and leads to second sound. The physics of superconductors is complicated by the *charge* of the Cooper pairs and by the coupling of electron motion to the underlying ionic lattice. Low energy phase-degrees of freedom are still important, although now it is the vector potential which acquires a mass via the usual Higgs mechanism.

The excitations discussed above are all continuously connected to the ground state. However, point, line and wall defects in the order parameter texture, which are *not* continuously connected to the ground state, may also be important. Dislocation lines mediate plastic flow, and point-like vacancies and interstitials allow rapid particle diffusion in crystalline solids. Vortex rings control the decay of supercurrents in superfluids and superconductors. Most laboratory ferromagnets are subject to weak crystal fields, which break rotational invariance. In this case, the width of hysteresis loops below the Curie temperature is controlled by the motion of Bloch walls. Under some circumstances, such topological defects also play an important role in the phase transition out of the broken symmetry state.

In this review, we discuss the defects which arise in superfluids, superconductors and membranes. Although the emphasis is how to incorporate defects into simple Landau-Ginzburg field theories, we also touch upon their role in the statistical mechanics. We concentrate on two-dimensional systems, so that the defects are typically point-like.

The classic example of vortices and the Kosterlitz-Thouless transition in superfluid helium films is discussed first, together with universal jump in the superfluid density. Experimental confirmation of this prediction was an important test of the idea of defect-mediated

phase transitions. *Screening* of defect energies in superconducting films is then treated, with particular attention to the spreading of magnetic field lines in the three-dimensional volume outside the sample. When this spreading is ignored, screening efficiently cuts off the logarithmic divergence in the vortex energy. The finite energy vortices in this “naive” theory then proliferate for entropic reasons at any finite temperature, thus destroying superconductivity. In realistic samples, however, magnetic field line spreading (which arises because supercurrents are confined to a two-dimensional plane) renders screening less efficient, and a Kosterlitz-Thouless transition from a finite temperature superconducting state becomes possible.

The remainder of the paper contrasts the behavior of defects in membranes and monolayers. By “monolayers,” we mean crystalline films strongly confined to a plane. Dislocations and disclinations control the statistical mechanics of monolayers in a way similar to vortices in neutral superfluids. Successive dislocation and disclination unbinding transitions lead from crystalline to hexatic to liquid monolayer phases. In contrast to monolayers, “membranes” have a relatively low energy cost to buckle out of the two-dimensional plane, thus escaping into the third dimension. As a result, defects can be screened by out-of-plane displacements much like vortices in the “naive” model of superconducting films. Dislocations, for example, now have a finite energy. Their entropic proliferation causes crystals to be replaced by *hexatics* as the inevitable low temperature phase of membranes. We also discuss the buckling of 5- and 7-fold disclinations, of vacancies, interstitial and impurity atoms, and of grain boundaries.

We conclude by emphasizing the fundamental asymmetry between 5- and 7-fold disclinations in membranes. There is an exact symmetry between plus and minus vortices in superfluids and between dislocations with equal and opposite burgers vectors in two-dimensional crystals, which forces the energies of the defect and anti-defects to be equal. No such symmetry, however, insures that the core energies of plus and minus disclinations are identical. These disclinations represent points of local 5- and 7-fold coordination, where the number of neighboring particles is determined by the Dirichlet construction. This situation is similar to vacancies and interstitials in crystalline solids: Vacancies typically have a lower energy than interstitials, even though these excitations are “anti-defects” of each other.

Disclination asymmetry is of little consequence in flat monolayers, where the concentrations of 5- and 7-fold defects must be equal for topological reasons. (More precisely, Euler’s theorem ensures that the average coordination is six in a sufficiently large system.) In hexatic monolayers, moreover, the logarithmic divergences in the energies of isolated plus and minus disclinations have equal coefficients. The situation is different, however, in *membranes*

which are free to change their topology or with free boundary conditions which allow them to curl up near the edges. When the bending rigidity which controls out-of-plane fluctuations is small, buckling in hexatic membranes leads to different coefficients in the logarithmically diverging disclination energies. In liquid membranes, moreover, different core energies of plus and minus disclinations will inevitably bias the system towards a net positive or negative average Gaussian curvature. The energy asymmetry between 5- and 7-fold disclinations in the liquid determines the sign of the Gaussian rigidity, which acts as chemical potential controlling their population difference. Returning to the comparison with a superconductor, the Gaussian rigidity acts like an external magnetic field, which would bias superconducting films toward a net excess of plus or minus vortices. In membranes, the sign of the Gaussian bending rigidity determines whether vesicle phases (with positive net Gaussian curvature) or “plumbers nightmare” phases (with overall negative Gaussian curvature) are preferred.

Theories and simulations of hexatic and liquid membranes usually avoid this issue by imposing a definite spherical or toroidal topology, which automatically fixes the difference in the number of 5- and 7-fold defects. Such constraints are clearly artificial, however, for lipid bilayer membranes which can change their topology at will, and may even have free edges at some intermediate stage of a topological change. The analogous constraint for vacancies and interstitials in solids would be imposed by periodic boundary conditions: these defects can then only be created in pairs. In real solids, with free boundary conditions, vacancies and interstitials can enter at the surface to produce the concentrations dictated by the microscopic energetics. The simplest probe of disclination bias would be to simulate liquid membranes with free edges, and see which defect begins to dominate as the bending rigidity is reduced from large values. See section III.D for details.

II. TWO-DIMENSIONAL SUPERFLUIDS AND SUPERCONDUCTORS

A detailed and successful theory of two-dimensional superfluidity was constructed in the 1970s. The theory explains the observed properties of thin films of superfluid He⁴ on various substrates and the physics of thin superconducting films. The basic physical idea of defect unbinding was proposed by Kosterlitz and Thouless [1], by Berezinski [2], and, in a different physical context, by deGennes [3]. The first detailed calculations were carried out by Kosterlitz [4], who exploited a pioneering renormalization group method developed by Anderson and Yuval for the Kondo problem [5]. Because extensive reviews are available elsewhere [6–8], we limit ourselves to a brief sketch of the models and the basic results. We shall see how vortices control the basic physics and discuss their statistical mechanics.

We discuss only equilibrium properties, and ignore the important area of superfluid and superconducting dynamics [9,10].

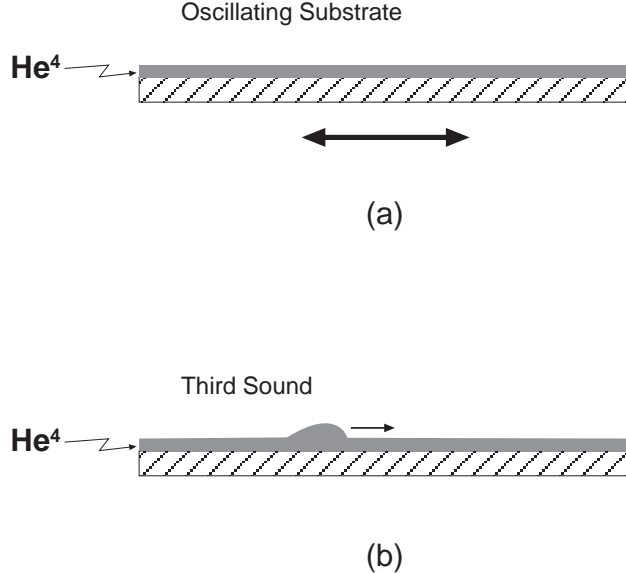


FIG. 1. (a) Schematic of an oscillating substrate experiment, which measures the superfluid density. (b) Propagation of a third sound excitation. Measuring the dispersion relation also allows one to extract $\rho_s(T)$.

A. Superfluid Helium Films: Experimental Facts

Superfluidity arises with decreasing temperature in helium films in a fundamentally different way than in bulk materials. Two basic experiments which reveal this difference are illustrated in Fig. 1. On an oscillating substrate, a finite fraction of the He^4 film decouples from the underlying motion below a critical temperature T_c . The film appears lighter than it should be, and measuring this deficit allows one to extract the temperature-dependent superfluid density $\rho_s(T)$ [11]. In a related experiment, third-sound excitations similar to capillary waves propagate below T_c with negligible damping through films as thin as a fraction of an Angstrom [12]. Such propagating waves would be impossible in a classical fluid, due to viscous damping. The primary restoring force is the Van der Waals attraction to the substrate (rather than gravity or surface tension), and again one can extract $\rho_s(T)$ provided the temperature is not too close to T_c , where the waves become strongly damped.

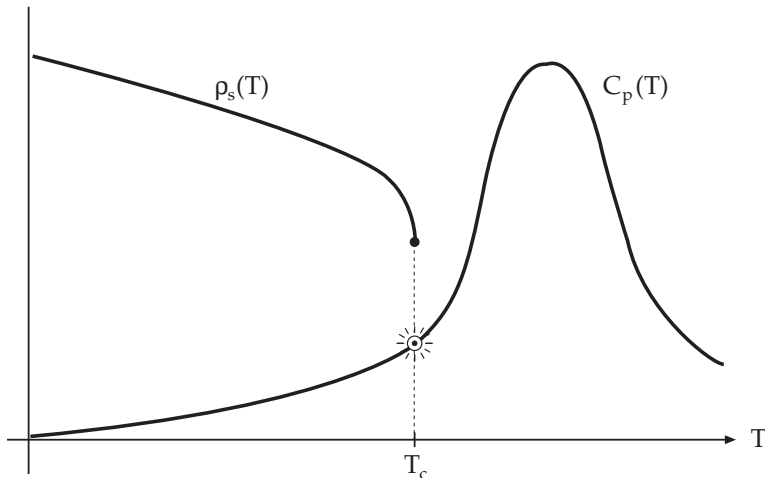


FIG. 2. Jump discontinuity in the superfluid density $\rho_s(T)$ as a function of temperature for a fixed thickness helium film. Also shown is the superfluid specific heat at constant pressure as a function of temperature. There is only an essential singularity, $C_p(T) \approx c_1 + c_2 \exp[-c_3/|T - T_c|^{1/2}]$, near the transition, where the c_i are constants.

As illustrated in Fig. 2, the superfluid density in films actually jumps discontinuously to zero at T_c , in contrast to the continuous vanishing observed in bulk superfluid He^4 . The phase transition is nevertheless *not* first order, as becomes evident from an examination of the specific heat (see Fig. 3). There is only a rounded maximum *above* the transition temperature, in contrast to the delta function peak expected for a true first-order transition. The detailed theory shows that the specific heat contains only an unobservable essential singularity at the transition itself [14,13].

B. Theoretical Background

Understanding the equilibrium behavior of superfluid helium films at temperature T requires calculation of quantities such as the quantum partition function,

$$Z = \text{Tr}' \{ e^{-\hat{\mathcal{H}}/T} \}, \quad (2.1)$$

where \mathcal{H} is the Hamiltonian operator,

$$\hat{\mathcal{H}} = \frac{-\hbar^2}{2m} \sum_{j=1}^N \nabla_j^2 + \sum_{i>j} V(|\vec{r}_i - \vec{r}_j|), \quad (2.2)$$

and Tr' means a sum over all *symmetrized* energy eigenfunctions, reflecting the bosonic nature of a He^4 atom. Here $V(r)$ is the boson pair potential, and we have set Boltzmann's

constant $k_B = 1$. Explicit computation of Z for a fixed large number of particles N by finding all symmetric energy eigenfunctions (or even just the ground-state wave function [15]) is difficult and it is useful to bypass this problem by changing to a second quantized representation of the many body physics. In second quantized notation, the Hamiltonian (2.2) reads

$$\begin{aligned} \widehat{\mathcal{H}} &= \int d^3r \hat{\psi}^+(\vec{r}) \left(\frac{-\hbar^2}{2m} \nabla^2 \right) \hat{\psi}(\vec{r}) \\ &+ \frac{1}{2} \int d^3r \int d^3r' \hat{\psi}^+(\vec{r}) \hat{\psi}^+(\vec{r}') V(|\vec{r} - \vec{r}'|) \hat{\psi}(\vec{r}') \hat{\psi}(\vec{r}) , \end{aligned} \quad (2.3)$$

where $\hat{\psi}^+(\vec{r})$ and $\hat{\psi}(\vec{r})$ are boson creation and destruction operators obeying the commutation relations,

$$[\hat{\psi}(\vec{r}), \hat{\psi}^+(\vec{r}')] = \delta(\vec{r} - \vec{r}') , \quad (2.4)$$

with all other commutators zero. Within the second quantization formalism, it is convenient to calculate thermodynamic quantities via the *grand* canonical partition function,

$$Z_{gr} = Tr' \left\{ e^{-(\widehat{\mathcal{H}} - \mu \widehat{N})/T} \right\} , \quad (2.5)$$

where μ is the chemical potential and the number operator is

$$\widehat{N} = \int d^3r \hat{\psi}^+(\vec{r}) \hat{\psi}(\vec{r}) . \quad (2.6)$$

As pointed out by Penrose and Onsager [16], Bose condensation in bulk He^4 is associated with off-diagonal long-range order in the correlation function,

$$G(r) = \langle \psi^+(\vec{r}) \psi(\vec{0}) \rangle , \quad (2.7)$$

where $\langle Q \rangle$ means $Tr' \{ Q \exp[-(\widehat{\mathcal{H}} - \mu \widehat{N})/T] \} / Z_{gr}$. Specifically, one has

$$\begin{aligned} \lim_{r \rightarrow \infty} G(r) &= \langle \hat{\psi}^+(\vec{r}) \rangle \langle \hat{\psi}(\vec{0}) \rangle \\ &\neq 0 . \end{aligned} \quad (2.8)$$

A simplified description of superfluidity in terms of a *Landau* theory results from a coarse graining procedure. In the case of helium films, we start by defining a *c*-number field

$$\psi(\vec{r}) = \langle \hat{\psi} \rangle_{\Omega(\vec{r})} , \quad (2.9)$$

where the brackets include a spatial average over a volume $\Omega(\vec{r})$ centered on \vec{r} which is large compared to the spacing between helium atoms but small compared to the overall system

size. The coarse-grained fields $\psi^*(\vec{r})$ and $\psi(\vec{r})$ (which are nonzero when the He⁴ liquid is superfluid in view of Eq. (2.8)) behave like complex numbers (instead of operators) for large enough averaging volumes. In helium films, we also take the averaging size to be large compared to the film thickness. The long wavelength spatial configurations of the system are now specified by complexions of $\psi(\vec{r})$, where \vec{r} is a *two*-dimensional spatial variable, and the partition function is a functional integral,

$$Z_{gr} = \int \mathcal{D}\psi(\vec{r}) \exp[-F/T] . \quad (2.10)$$

The free energy F includes entropic contributions due to the coarse-graining procedure. The Landau expansion of F/T in the order parameter $\psi(r)$ has the same form as $\widehat{\mathcal{H}} - \mu\widehat{N}$, with $\widehat{\psi}(\vec{r})$ and $\widehat{\psi}^+(\vec{r})$ replaced by the *c*-number fields $\psi(\vec{r})$ and $\psi^*(\vec{r})$,

$$\frac{F}{T} = \int d^2r \left[\frac{1}{2} A |\vec{\nabla}\psi|^2 + \frac{1}{2} a |\psi|^2 + b |\psi|^4 + \dots \right] \quad (2.11)$$

where, as usual, a changes sign at the mean-field transition temperature T_c^0 , $a = a'(T - T_c^0)$.

Because the long wavelength fluctuations in a helium film are two-dimensional, the actual temperature T_c where true long-range order develops is suppressed well below T_c^0 . For $T \approx T_c$, $a \ll 0$ and the polynomial part of F has a deep minimum, even though thermal fluctuations may nevertheless suppress genuine diagonal long-range order at the largest length scales. To a first approximation, we can then neglect fluctuations in the *amplitude* of $\psi(r)$, and set

$$\psi(\vec{r}) \approx \psi_0 e^{i\theta(\vec{r})}, \quad (2.12)$$

where $\psi_0 \approx \sqrt{-a/4b}$ and $\theta(\vec{r})$ is a slowly varying phase variable. The free energy becomes

$$\frac{F}{T} = \text{const.} + \frac{1}{2} K_0 \int |\vec{\nabla}\theta(\vec{r})|^2 d^2r, \quad (2.13)$$

where $K_0 = A\psi_0^2$. The physical interpretation of K_0 becomes clear if we recall that the superfluid velocity \vec{v}_s is given by [17]

$$\vec{v}_s(\vec{r}) = \frac{\hbar}{m} \vec{\nabla}\theta(\vec{r}), \quad (2.14)$$

and write the contribution to F of the superfluid kinetic energy in terms of the superfluid density ρ_s^0 as

$$F = \text{const.} + \frac{1}{2} \rho_s^0 \int d^2r |\vec{v}_s(\vec{r})|^2 . \quad (2.15)$$

Evidently, K_0 is related to the superfluid density in this “phase only” approximation by

$$K_0 = \frac{\hbar^2}{m^2 T} \rho_s^0 . \quad (2.16)$$

The peculiar nature of superfluid order in two dimensions becomes evident if we now evaluate $G(r)$, by integrating freely over the phase field when evaluating averages weighted by $e^{-F/T}$,

$$\begin{aligned} G(r) &= \langle \psi(\vec{r}) \psi^*(\vec{0}) \rangle \\ &= \psi_0^2 \exp \left[-\frac{1}{2} \langle [\theta(\vec{r}) - \theta(\vec{0})]^2 \rangle \right] , \end{aligned} \quad (2.17)$$

where the last line is a general property of Gaussian fluctuations. Upon introducing Fourier variables, the remaining average is easily evaluated using the equipartition theorem,

$$\begin{aligned} \langle [\theta(\vec{r}) - \theta(\vec{0})]^2 \rangle &= \frac{2}{K_0} \int \frac{d^2 q}{(2\pi)^2} \frac{1}{q^2} (1 - e^{i\vec{q}\cdot\vec{r}}) \\ &\underset{r \rightarrow \infty}{\approx} \frac{1}{K_0} \ln(r/a_0) , \end{aligned} \quad (2.18)$$

where a_0 is a microscopic cutoff. We thus find that $G(r)$ decays *algebraically* to zero [18],

$$G(r) \sim 1/r^{\eta(T)} , \quad (2.19)$$

with

$$\eta(T) = 1/2\pi K_0(T) . \quad (2.20)$$

Thus there is only *quasi*-long range off-diagonal long-range order at any finite temperature in two dimensions. Nevertheless, this algebraic order is enough to distinguish the low-temperature superfluid from a distinct high temperature normal liquid film in which $G(r)$ decays exponentially,

$$G(r) \sim \exp[-r/\xi(T)] , \quad (2.21)$$

which defines a superfluid coherence length $\xi(T)$. Note that the low-temperature phase still has a nonzero superfluidity density, similar to bulk superfluids. In contrast to bulk superfluids, however, the low-temperature phase is characterized by a *continuously varying* critical exponent $\eta(T)$.

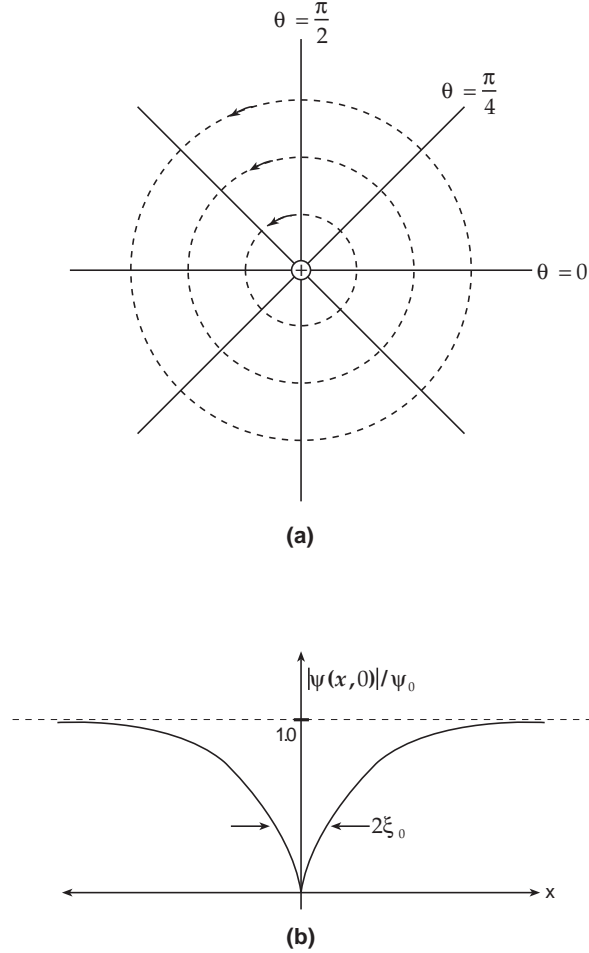


FIG. 3. (a) Lines of constant phase associated with a vortex in a two-dimensional superfluid. Dashed circles are the streamlines for the associated supercurrents. (b) Variation of the order parameter magnitude near a vortex core located at the origin.

The “phase only” description used above neglects amplitude fluctuations, and ignores the periodic nature of the phase variable. We can account for both effects by introducing a discrete set of vortex singularities in $\psi(\vec{r})$. As illustrated in Fig. 3a, vortices represent zeroes of $\psi(\vec{r})$, where the phase is undetermined. Near a vortex core, the assumption that the order parameter amplitude $|\psi(\vec{r})|$ is a constant breaks down. Fig. 3b shows how $\psi(\vec{r})$ varies in the vicinity of a vortex [19]. $\psi(\vec{r})$ rises from zero to its bulk value over a characteristic length ξ_0 , related to the coefficients of the first two terms of Eq. (2.11),

$$\xi_0 = \sqrt{A/|a|} . \quad (2.22)$$

To describe a radially symmetric net phase change of $\pm 2\pi$ near a vortex centered at the origin, we set

$$\theta(x, y) = \pm \tan^{-1}(y/x) . \quad (2.23)$$

According to Eq. (2.14) we then have a velocity field

$$\vec{v}_s = \frac{\hbar}{m} \frac{\hat{z} \times \vec{r}}{r^2} , \quad (2.24)$$

which leads to a vortex energy

$$E_v = \pi \rho_s^0 \frac{\hbar^2}{m^2} \ln(R/\xi_0) + C \quad (2.25)$$

when inserted into Eq. (2.15), where, R is the system size. We have imposed a lower cutoff ξ_0 and included the contribution from smaller scales where the amplitude varies in the constant C . Since there are approximately $(R/\xi_0)^2$ distinct positions for a vortex, the *free* energy $E_v - TS_v$ for large R is

$$F_v \approx \left(\pi \rho_s^0 \frac{\hbar^2}{m^2} - 2T \right) \ln(R/\xi_0) . \quad (2.26)$$

The prediction of this famous argument [1–3] is that it becomes favorable for vortices to proliferate (leading to exponential decay of $G(r)$) above a critical temperature

$$T_c \approx \frac{\pi \hbar^2}{2 m^2} \rho_s^0 . \quad (2.27)$$

C. Vortex Statistical Mechanics and Renormalization of ρ_s

Going beyond the simple argument presented above requires a more detailed theory, which allows for a finite density of interacting vortices near T_c . Understanding superfluidity in two-dimensional helium films is equivalent to solving the statistical mechanics of this vortex gas. We start by noticing that functional integrals like the partition function (2.10) are dominated in the low-temperature “phase only” approximation by solutions of

$$\nabla^2 \theta = 0 . \quad (2.28)$$

To allow for vortices (and thus for amplitude fluctuations), we require that Eq. (2.28) be satisfied “almost everywhere,” i.e., everywhere except in the cores of a collection N of vortices located at positions $\{\vec{r}_\alpha\}$ with integer charges $\{s_\alpha\}$. A vortex singularity has “charge” s_α if the line integral of the phase gradient on any path enclosing the core satisfies,

$$\oint \vec{\nabla} \theta \cdot d\vec{\ell} = 2\pi s_\alpha . \quad (2.29)$$

The function (2.23) obeys this condition, for example, with $s_\alpha = \pm 1$. More generally we expect, for a contour \mathcal{C} enclosing many vortices, that

$$\oint_{\mathcal{C}} \vec{\nabla}\theta \cdot d\ell = \int_{\Omega} d^2r n_v(\vec{r}) , \quad (2.30)$$

where Ω is the area spanned by \mathcal{C} and the vortex “charge density” is

$$n_v(\vec{r}) = 2\pi \sum_{\alpha=1}^N s_\alpha \delta(\vec{r} - \vec{r}_\alpha) . \quad (2.31)$$

Equation (2.30) is a statement about the noncommutivity of derivatives of $\theta(x, y)$. Indeed, by taking the contour \mathcal{C} to be a small square loop, we readily find

$$\begin{aligned} \epsilon_{ij} \partial_i \partial_j \theta(\vec{r}) &= \partial_x \partial_y \theta - \partial_y \partial_x \theta \\ &= n_v(\vec{r}) , \end{aligned} \quad (2.32)$$

where ϵ_{ij} is the antisymmetric unit tensor in two dimensions, $\epsilon_{xy} = -\epsilon_{yx} = 1$. To cast this equation in a more familiar form, we introduce the Cauchy conjugate to the phase field, by

$$\partial_i \theta(\vec{r}) = \epsilon_{ij} \partial_j \tilde{\theta}(\vec{r}) , \quad (2.33)$$

and find that $\tilde{\theta}(x, y)$ satisfies

$$\nabla^2 \tilde{\theta}(\vec{r}) = n_v(\vec{r}) . \quad (2.34)$$

Finding the phase associated with a set of vortex singularities thus requires that we first determine the “electrostatic potential” $\tilde{\theta}(\vec{r})$ of a collection of point charges $\{s_j\}$ at positions $\{\vec{r}_j\}$ in two dimensions [1]. The solution of Eq. (2.34) is

$$\tilde{\theta}(\vec{r}) = 2\pi \sum_{\alpha} s_\alpha G(\vec{r}, \vec{r}_\alpha) , \quad (2.35)$$

where the Green’s function satisfies

$$\nabla^2 G(\vec{r}, \vec{r}_\alpha) = \delta(\vec{r} - \vec{r}_\alpha) . \quad (2.36)$$

For $|\vec{r} - \vec{r}_j|$ large and both points far from any boundaries, we have

$$G(\vec{r}, \vec{r}_j) \approx \frac{1}{2\pi} \ln \left(\frac{|\vec{r} - \vec{r}_j|}{\xi_0} \right) + C , \quad (2.37)$$

where C is a constant which contributes to the vortex core energy.

We now decompose the phase into a contribution $\theta_v(x, y)$ from vortices, obtained by taking the Cauchy conjugate of Eq. (2.35), and a smoothly varying part $\phi(x, y)$,

$$\theta(x, y) = \theta_v(x, y) + \phi(x, y) . \quad (2.38)$$

The function $\phi(x, y)$ represents single-valued phase fluctuations superimposed on the vortex extrema. Thermodynamic averages are obtained by first integrating over this nonsingular phase field, and then summing over all possible complexions of vortex charges and positions. To insert this decomposition into Eq. (2.13), we need

$$\vec{\nabla}\theta(\vec{r}) = 2\pi(\hat{z} \times \vec{\nabla}) \int d^2r' n(\vec{r}') G(\vec{r}, \vec{r}') + \vec{\nabla}\phi . \quad (2.39)$$

The resulting free energy takes the form [1]

$$\frac{F}{T} = \text{const.} + \frac{1}{2}K_0 \int d^2r |\vec{\nabla}\phi|^2 + \frac{F_v}{T} , \quad (2.40)$$

where the vortex part is

$$\frac{F_v}{T} = -\pi K_0 \sum_{\alpha \neq \beta} s_\alpha s_\beta \ln \left(\frac{|\vec{r}_\alpha - \vec{r}_\beta|}{a} \right) + \frac{E_c}{T} \sum_\alpha s_\alpha^2 , \quad (2.41)$$

and the core energy E_c is usually assumed to be proportional to K_0 . Implicit in the statistical mechanics associated with Eq. (2.41) is a constraint of overall ‘‘charge neutrality,’’ $\sum_j s_j = 0$, required for a finite energy in the thermodynamic limit.

D. Renormalization Group and Universal Jump in the Superfluid Density

To illustrate the statistical mechanics of the vortex gas described above, consider the renormalized superfluid density $\rho_s^R(T)$ calculated to lowest order in the vortex fugacity

$$y = e^{-E_c/T} . \quad (2.42)$$

The renormalized superfluid density is related to the correlations of the momentum density $\vec{g}(\vec{r})$. On a microscopic level, the momentum density operator $\hat{g}_i(\vec{r})$ is given in terms particle creation and destruction operators by

$$\hat{g}_i(\vec{r}) = \frac{\hbar}{2i} \left[\hat{\psi}^+(\vec{r}) \partial_i \hat{\psi}(\vec{r}) - \hat{\psi}(\vec{r}) \partial_i \hat{\psi}^+(\vec{r}) \right] . \quad (2.43a)$$

When local off-diagonal long-range order is present in helium films, we replace $\hat{\psi}^+(\vec{r})$ and $\hat{\psi}(\vec{r})$ by coarse-grained two-dimensional classical c -number fields, as usual. In the ‘‘phase only’’ approximation which led to Eq. (2.13), the coarse-grained momentum density is then

$$\vec{g}(\vec{r}) = \rho_s^0 \vec{v}_s(\vec{r}) , \quad (2.43b)$$

where $\rho_s^0 = m|\psi_0|^2$, and $\vec{v}_s(\vec{r})$ includes possible contributions from vortices. In helium films, the contribution of the *normal* fluid to the momentum vanishes, due to the viscous coupling to the substrate.

The correlation matrix which determines the renormalized superfluid density is

$$C_{ij}(\vec{q}, K, y) \equiv \langle g_i(\vec{q})g_j^*(\vec{q}) \rangle, \quad (2.44a)$$

where $g_i(\vec{q})$ is the Fourier transform of the i -th component of $\vec{g}(\vec{r})$. To extract the renormalized superfluid density, we first decompose C_{ij} into transverse and longitudinal parts:

$$C_{ij} = A(q)\frac{q_i q_j}{q^2} + B(q)\left(\delta_{ij} - \frac{q_i q_j}{q^2}\right). \quad (2.44b)$$

In an isotropic classical liquid, one would have $A(q) = B(q)$ in the limit $q \rightarrow 0$. The momentum fluctuations, moreover, would decouple from the configurational degrees of freedom responsible for most phase transitions. The behavior of quantum fluids is different: The renormalized superfluid density $\rho_s^R(T)$, in particular, is given by the difference between A and B as q tends to zero (see Appendix)

$$\rho_s^R(T) = \frac{1}{T} \lim_{q \rightarrow 0} [A(q) - B(q)]. \quad (2.45)$$

The momentum density $\vec{g}(\vec{r}) = \rho_s \frac{\hbar}{m} \vec{\nabla} \theta(\vec{r})$ is already decomposed into transverse and longitudinal parts in Eq. (2.39). One readily finds that C_{ij} takes the form (2.44b), with [8]

$$\frac{\hbar^2}{m^2 T} A(q) = K_0 \quad (2.46a)$$

$$\frac{\hbar^2}{m^2 T} B(q) = \frac{4\pi^2 K_0^2}{q^2} \langle \hat{n}_v(\vec{q}) \hat{n}_v(-\vec{q}) \rangle. \quad (2.46b)$$

where $\hat{n}_v(\vec{q})$ is the Fourier transform of the vortex density $n_v(\vec{r})$, and the average in (2.46b) is to be carried out over the vortex part of the free energy.

When the vortices are dilute, it is straightforward to use these results to obtain a fugacity perturbation expansion for the renormalized superfluid density. In terms of $K_R \equiv \hbar^2 \rho_s^R / m^2 T$, we have [8]

$$K_R^{-1} = K_0^{-1} + 4\pi^3 y_0^2 \int_a^\infty \frac{dr}{a} \left(\frac{r}{a}\right)^{3-2\pi K_0} + O(y_0^4). \quad (2.47)$$

At low temperatures, Eq. (2.47) provides a small correction (proportional to $e^{-2E_c/T}$) to K_R^{-1} . When $K_0 \lesssim 2/\pi$, however, the integral becomes infrared divergent and perturbation theory breaks down. This is precisely the condition (2.27) required for a vortex unbinding transition. This potentially divergent perturbation theory can be converted into renormalization group

recursion relations for effective couplings $K(\ell)$ and $y(\ell)$ describing renormalized vortices with effective core diameter $ae^{-\ell}$. These differential equations read

$$\frac{dK^{-1}(\ell)}{d\ell} = 4\pi^2 y^2(\ell) + O[y^4(\ell)] , \quad (2.48a)$$

$$\frac{dy(\ell)}{d\ell} = [2 - \pi K(\ell)]y(\ell) + O[y^3(\ell)] . \quad (2.48b)$$

Another important result is the invariance of the superfluid density along a renormalization group trajectory,

$$K_R(K, y) = K_R(K(\ell), y(\ell)) , \quad (2.49)$$

where $K_R(K, y) = \frac{\hbar^2}{m^2 T} \rho_s^R(K, y)$. This result also follows from the Josephson scaling relation for ρ_s^R [23].

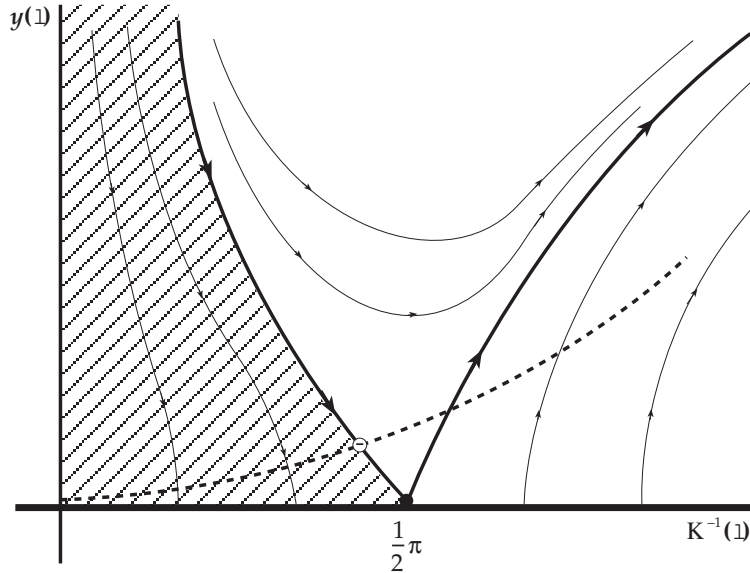


FIG. 4. Renormalization flows arising from the Kosterlitz recursion relations. The shaded domain of attraction of the fixed line at $y(\ell) = 0$ is a superfluid. A locus of initial conditions is shown as a dashed line. The superfluid phase is bounded by the incoming separatrix which terminates at $K^{-1} = 2/\pi$.

Equations (2.48) are the famous Kosterlitz recursion relations, originally derived by him using another method [4]. The Hamiltonian trajectories they generate in the (K^{-1}, y) -plane are shown in Fig. 4, together with a temperature-dependent locus of initial conditions,

$$y_0 = e^{-cK_0} , \quad (2.50)$$

where c is a constant.

Initial conditions to the left of the incoming separatrix renormalize into the line of fixed points at $y = 0$, which describes the low-temperature phase. At higher temperatures, $y(\ell)$ eventually becomes large, indicating that vortices unbind at long wavelengths. One then expects that order parameter correlations decay exponentially, as in Eq. (2.21), where the correlation length ξ_+ is related to the density of free vortices n_f :

$$n_f(T) \approx \xi_+^{-2}(T). \quad (2.51)$$

A variety of detailed predictions for the Kosterlitz-Thouless transition follow from these recursion relations and the transformation properties of various correlation functions under the renormalization group [4]. We focus here on the prediction of a *universal* jump discontinuity in the superfluid density [23]. This is a direct consequence of the relation (2.49) and the renormalization group flows shown in Fig. 4. Below T_c , $y(\ell)$ tends to zero for large ℓ , and we have

$$\begin{aligned} K_R(K, y) &= \lim_{\ell \rightarrow \infty} K_R(K(\ell), y(\ell)) \\ &= \lim_{\ell \rightarrow \infty} K(\ell) \quad (T \lesssim T_c). \end{aligned} \quad (2.52)$$

Since it is clear from Fig. 4 that this limit is just $2/\pi$, at T_c , we have

$$\lim_{T \rightarrow T_c^-} K_R(K, y) = \lim_{T \rightarrow T_c^-} \frac{\hbar^2 \rho_s^R(T)}{m^2 T} = \frac{2}{\pi}, \quad (2.53)$$

independent of the way in which the initial locus crosses the incoming separatrix. In helium films of varying thickness on varying substrates, one predicts a sequence of curves with jump discontinuities and T_c values all falling on a line with slope

$$\frac{\rho_s(T_c^-)}{T_c^-} = \frac{2m^2}{\pi \hbar^2 k_B T} \approx 3.491 \times 10^{-9} \text{ g cm}^{-2} \text{ K}^{-1}. \quad (2.54)$$

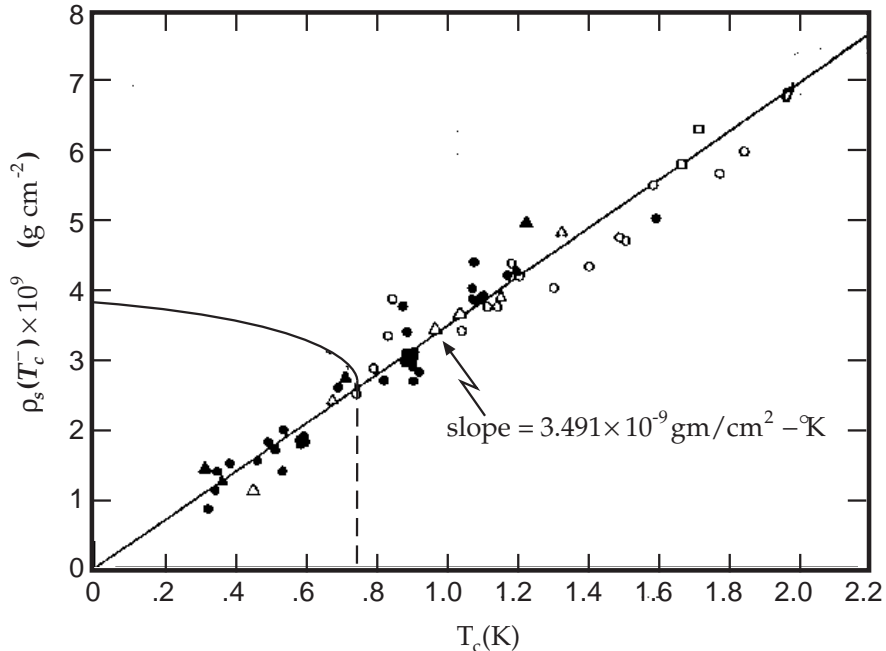


FIG. 5. Jump discontinuities in the superfluid density vs. temperature for over 70 different experiments for helium films. One representative $\rho_s(T)$ curve is shown. Adapted from Ref. [11].

Fig. 5 shows the locus of jump discontinuities in the superfluid density vs. temperature for over 70 experiments on helium films. All points lie on a line with slope close to the universal value (2.54). This remarkable universal jump is related to the universality of the critical exponent $\eta(T)$ at the Kosterlitz-Thouless transition. When vortices are taken into account, $G(r) \sim \frac{1}{r^{\eta(T)}}$ for $T < T_c$, provided Eq. (2.20) is replaced by [4]

$$\eta(T) = 1/2\pi K_R(T) , \quad (2.55)$$

so that (neglecting logarithmic corrections) $\eta(T_c^-) = 1/4$.

E. Two-Dimensional Superconductors

Superconducting films are similar to substrates coated with superfluid He⁴, with the understanding that the complex order parameter $\psi(\vec{r})$ describes Cooper pairs of electrons. Because the bosonic degrees of freedom are now charged, the currents surrounding vortices are screened by a coupling to the vector potential. The interactions between vortices are no longer logarithmic at all distances, but instead die off rapidly at scales larger than the London penetration depth. We first review a “naive” theory of screening in two-dimensional

superconductors. This theory is “two-dimensional” in the sense that all quantities are independent of the z coordinate. It would be directly applicable to situations in which vortices are, in effect, infinitely long rigid rods in a *bulk* material, and no thermal variation in the phase or vortex positions allowed along the z axis. The conclusion of the naive theory is that, due to screening, vortices will always unbind at any nonzero temperature [1]. We then discuss real superconducting films, which behave differently, due to the spreading of the vortex magnetic field lines (see Fig. 6) as they emerge from the top and bottom of the film [24]. As emphasized by Beasley *et al.* [25] vortices in sufficiently thin superconducting films now interact logarithmically out to an *effective* London penetration depth of order millimeters, and the Kosterlitz-Thouless theory for neutral superfluids becomes directly applicable over a wide range of length scales in most samples. The detailed predictions of the Kosterlitz-Thouless theory when transcribed to superconducting films are discussed in Ref. [10].

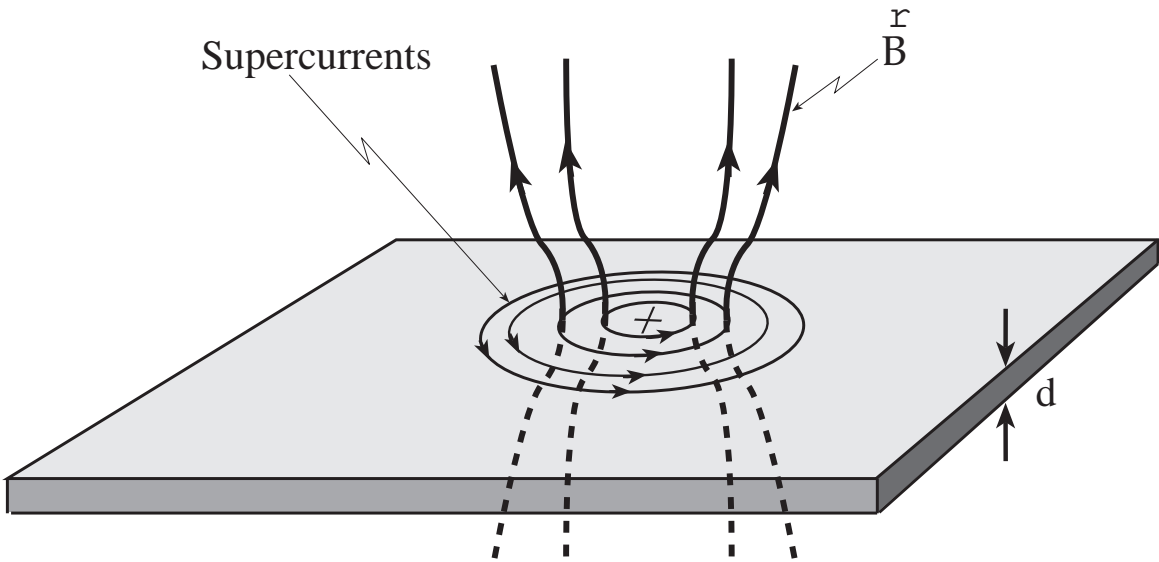


FIG. 6. Schematic of currents and magnetic field lines for a vortex in a superconducting film. Currents only flow in a two-dimensional plane, so the screening is weak.

We begin with the “naive” theory of two-dimensional superconductors because it provides a simple illustration of the screening of defect interactions by a vector potential. A closely related, but nonlinear screening phenomenon arises for dislocations in membranes (see Sec. III), and leads to the striking conclusion that crystalline membranes must *always* melt into hexatic liquids at any finite temperature.

1. Naive Theory

We start with Ginzburg-Landau theory of superconductivity [26], which generalizes Eq. (2.11) for neutral superfluids to charged Cooper pairs,

$$F = \int d^2r \left[\frac{1}{2m^*} \left| \left(\frac{\hbar}{i} \vec{\nabla} - \frac{e^*}{c} \vec{A} \right) \psi \right|^2 + \frac{1}{2} r |\psi|^2 + u |\psi|^2 + \frac{B^2}{8\pi} - \frac{1}{4\pi} \vec{H} \cdot \vec{B} \right]. \quad (2.56)$$

Here, $\psi(\vec{r})$ is a coarse-grained complex field which represents the microscopic Cooper pair destruction operator ($\psi^*(\vec{r})$ is the coarse-grained pair creation operator), $\vec{A}(\vec{r})$ is the vector potential, $e^* = 2e$ is the pair charge and $m^* = 2m$ is the effective mass of the pair. \vec{H} is a constant external field, and $\vec{B}(\vec{r}) = \vec{\nabla} \times \vec{A}(\vec{r})$ is fluctuating local magnetic field. Equation (2.56) is incorrect for real superconducting films because it implicitly assumes that *both* $\psi(\vec{r})$ and $\vec{A}(\vec{r})$ vanish outside the thin slab occupied by the superconductor. This is a reasonable assumption for $\vec{\psi}(\vec{r})$, but incorrect for $\vec{B}(\vec{r})$ and $\vec{A}(\vec{r})$. This theory does, however, describe a bulk superconductor which is infinitely stiff in the \hat{z} -direction, so that all quantities are independent of z . Equation (2.56) should then be interpreted as a free energy per unit length. A related theory provides the correct description of local order in two-dimensional smectic liquid crystals [27].

Let us see what Eq. (2.56) predicts for superconductors, with the external magnetic field \vec{H} set to zero. The modifications introduced by the fluctuating magnetic field $\vec{B}(\vec{r})$ outside the sample will be discussed in the next subsection. Following our treatment of helium films we assume that thermal excitations have suppressed any possible ordering well below the mean field transition temperature, so that $r \ll 0$. We again make the “phase only” approximation, and write

$$\psi(\vec{r}) = \psi_0 e^{i\theta(\vec{r})}, \quad (2.57)$$

with $\psi_0 = \sqrt{-r/4u}$. The two terms quadratic in $\psi(\vec{r})$ determine the superconducting coherence length,

$$\xi_0 = \sqrt{\hbar^2/m^*|r|}, \quad (2.58)$$

which is the length over which the order parameter rises from zero near a vortex. On scales larger than ξ_0 , so that the phase only approximation is valid, free energy becomes

$$F = \text{const.} + \int d^2r \left[\frac{1}{2} \rho_s^0 \left(\frac{\hbar}{m^*} \right)^2 \left| \vec{\nabla} \theta - \frac{e^*}{\hbar c} \vec{A} \right|^2 + \frac{1}{8\pi} |\vec{\nabla} \times \vec{A}|^2 \right], \quad (2.59)$$

where

$$\rho_s^0 = m^* |\psi_0|^2 \quad (2.60)$$

is the mass density of the Cooper pairs.

To see qualitatively how the vector potential affects the behavior of vortices, imagine that the vortex solution (2.23) for the phase variable is inserted in Eq. (2.59). Since $|\vec{\nabla} \theta| \sim 1/r$, this would lead to a logarithmically diverging energy, if the vector potential were neglected. The vector potential, however, will cancel out this divergence and reduce the energy provided it too falls off like $1/r$ with the correct coefficient far from the vortex. This screening costs gradient energy, however, due to the $|\vec{\nabla} \times \vec{A}|^2$ term. The two terms of Eq. (2.59) quadratic in \vec{A} become comparable when $\vec{A}(\vec{r})$ varies over a length scale λ_0 , with

$$\lambda_0 = \sqrt{\frac{(m^* c)^2}{\rho_s^0 4\pi (e^*)^2}}. \quad (2.61)$$

This scale is the London penetration depth, of order 1–10 thousand Angstroms in most superconductors. Because of this is the scale over which screening sets in, we expect the vortex energy to be finite and approximately equal to Eq. (2.25) with R replaced by λ_0 ,

$$E_v \approx \pi \rho_s^0 \left(\frac{\hbar}{m^*} \right)^2 \ln(c\lambda_0/\xi_0) \quad (2.62)$$

where c is an undetermined constant. Since the entropy of an isolated vortex is still proportional to $\ln R$, and the energy is now finite, we conclude that vortices will always be unbound in this model [1]. A more detailed analysis, similar to that for finite energy defects like vacancies and interstitials in a solid [28], predicts a nonzero density of free vortices

$$\eta_f \approx \xi_0^{-2} e^{-E_v/T} \quad (2.63)$$

at any temperature $T > 0$.

Because Eq. (2.59) is a simple quadratic form, we can go beyond the arguments sketched above, and determine the interactions between screened vortices in more detail. As in helium films, functional integrals weighted by $\exp[-F/T]$ will be dominated by vortex extrema of the free energy. In the Coulomb gauge, $\vec{\nabla} \cdot \vec{A} = 0$, the variational equation $\delta F/\delta \theta = 0$ again leads to $\nabla^2 \theta = 0$ away from the vortex cores, and we can immediately write down the vortex contribution to $\vec{\nabla} \theta$ from N vortices at position $\{\vec{r}_j\}$ with “charges” $\{s_j\}$,

$$\vec{\nabla}\theta(\vec{r}) = 2\pi \sum_{\alpha} s_{\alpha} (\hat{z} \times \vec{\nabla}) G(\vec{r}, \vec{r}_{\alpha}), \quad (2.64)$$

where $G(\vec{r}, \vec{r}_j)$ is the Green's function discussed in Section II.C above. Note from Eqs. (2.31) and (2.32) that the curl of $\vec{\nabla}\theta$ does not vanish,

$$\hat{z} \cdot (\vec{\nabla} \times \vec{\nabla}\theta) = 2\pi \sum_{\alpha} s_{\alpha} \delta^{(2)}(\vec{r} - \vec{r}_{\alpha}). \quad (2.65)$$

The vector potential is constrained by vortex singularities, even though $\theta(\vec{r})$ and $\vec{A}(\vec{r})$ appear to decouple in the Coulomb gauge. To see this, consider a closed path \mathcal{C} bounding an area Ω in the superconductor far compared to λ_0 from any vortex cores. On such a path the first term in (2.59) has been minimized, insuring that $\vec{\nabla}\theta = \frac{e^*}{\hbar c} \vec{A}$ and that

$$\oint_{\mathcal{C}} \left(\vec{\nabla}\theta - \frac{e^*}{\hbar c} \vec{A} \right) \cdot d\vec{\ell} = 0. \quad (2.66)$$

It then follows from Eq. (2.30) that the magnetic flux through Ω is given by the sum of the enclosed vortex ‘‘charges,’’

$$\iint_{\Omega} d^2r B_z = \phi_0 \sum_{\{r_{\alpha} \in \Omega\}} s_{\alpha}, \quad (2.67)$$

where $\phi_0 = \frac{2\pi\hbar c}{e^*}$ is the flux quantum.

A second variational equation follows from $\delta F/\delta \vec{A} = 0$, i.e.,

$$\vec{\nabla} \times [\vec{\nabla} \times \vec{A}(\vec{r})] = \vec{\nabla} \times \vec{B}(\vec{r}) = 4\pi\rho_s^0 \left(\frac{\hbar}{m^*} \right)^2 \left(\frac{e^*}{\hbar c} \right) \left(\vec{\nabla}\theta - \frac{e^*}{\hbar c} \vec{A}(\vec{r}) \right). \quad (2.68)$$

Upon casting this equation in the form of Ampere's law $\vec{\nabla} \times \vec{B}(\vec{r}) = 4\pi\vec{J}(\vec{r})/c$, we see that the (gauge invariant) supercurrent associated with θ and \vec{A} is

$$\vec{J}(\vec{r}) = e^* |\psi_0|^2 \frac{\hbar}{m^*} \left(\vec{\nabla}\theta(\vec{r}) - \frac{e^*}{\hbar c} \vec{A}(\vec{r}) \right). \quad (2.69)$$

Note the close analogy with the formula for the superfluid *momentum* density in helium films [29],

$$\vec{g}(\vec{r}) = m |\psi_0|^2 \frac{\hbar}{m} \vec{\nabla}\theta(\vec{r}). \quad (2.70)$$

A closed form equation for the magnetic field B_z generated by a distribution of vortices follows from taking the curl of Eq. (2.68), and using Eq. (2.65)

$$B_z - \lambda_0^2 \nabla_{\perp}^2 B_z = \phi_0 \sum_{\alpha=1}^N s_{\alpha} \delta^{(2)}(\vec{r} - \vec{r}_{\alpha}), \quad (2.71)$$

where “ \perp ” denotes coordinates in the plane of the film.

Consider one isolated vortex with charge s_α at the origin. The Fourier transformed field $B_z(\vec{q}_\perp)$ which solves Eq. (2.71) is then

$$B_z(\vec{q}) = \frac{s\phi_0}{1 + q_\perp^2 \lambda_0^2}, \quad (2.72)$$

which leads in real space to

$$B_z(r) = \frac{s\phi_0}{2\pi\lambda_0^2} K_0(r/\lambda_0), \quad (2.73)$$

where $K_0(x)$ is the Bessel function, $K_0(x) \approx \ln(1/x)$, $x \ll 1$, and $K_0(x) = \sqrt{\pi/2x} e^{-x}$, $x \gg 1$. The associated supercurrent $\vec{J}(r) = \vec{\nabla} \times \vec{B}(r)$ is

$$\vec{J}(\vec{r}) = \frac{sc\phi_0}{8\pi^2\lambda_0^3} K_1(r/\lambda_0) \hat{\theta}, \quad (2.74)$$

where $\hat{\theta}$ is a unit vector in the azimuthal direction. Note that $|\vec{J}(\vec{r})| \sim 1/r$ for $r \ll \lambda_0$, similar to the momentum density in helium films. However, screening sets in for $r \gg \lambda_0$, and $|\vec{J}(\vec{r})| \sim \exp(-r/\lambda_0)$. Similar manipulations lead straightforwardly to the generalization of the vortex-free energy (2.41) for two-dimensional charged superfluids,

$$F_v = \epsilon_0 \sum_{i \neq j} s_i s_j K_0\left(\frac{|\vec{r}_i - \vec{r}_j|}{\lambda_0}\right) + E_c \sum_j s_j^2, \quad (2.75)$$

where $\epsilon_0 = (\phi_0/4\pi\lambda_0)^2$ and E_c is a vortex core energy. Gaussian “spin wave” fluctuations about these vortex extrema can also be included [27]. The finite range of the interaction potential confirms our earlier conclusion that vortices will unbind for entropic reasons at any finite temperature in this model.

2. Real Superconducting Films

As illustrated in Fig. 6, the magnetic field lines generated by a vortex in real superconducting films spread out into the empty space above and below the plane of film. This spreading leads to different behavior for the screening currents in the film than that predicted by Eq. (2.74). The true behavior was first found by Pearl [24], and provides an interesting illustration of how two-dimensional physics can be effected by the outside, three-dimensional environment. We sketch the calculation here, following the treatment of deGennes [30].

Start by integrating Eq. (2.69) over a film of thickness d along \hat{z} . Provided the film is much thinner than the London penetration depth, we may assume that $\theta(\vec{r})$ and $\vec{A}_{2d}(\vec{r})$

remain constant across the film thickness. We denote the vector potential by $\vec{A}_{2d}(\vec{r})$ to emphasize that this quantity is the vector potential *in the two-dimensional film*, and not the full vector potential $\vec{A}_{3d}(\vec{r}, z)$ which describes the magnetic field in all of three-dimensional space. Note that $\vec{r} = (x, y)$ always refers to coordinates in the two-dimensional plane perpendicular to \hat{z} . If we imagine that all this current is concentrated in a delta function sheet in the plane $z = 0$, the full three-dimensional current may be written

$$\vec{J}(\vec{r}, z) = \frac{c}{4\pi} \frac{\phi_0}{2\pi\lambda_{\text{eff}}} \left[\vec{\nabla}\theta(\vec{r}) - \frac{2\pi}{\phi_0} \vec{A}_{2d}(\vec{r}) \right] \delta(z), \quad (2.76)$$

where

$$\lambda_{\text{eff}} = \lambda^2/d. \quad (2.77)$$

As we shall see, λ_{eff} will play the role of an effective London penetration depth in this problem.

The current (2.76) provides a source for a *three-dimensional* magnetic field $\vec{B}(\vec{r}, z)$ via Ampere's law, $\vec{\nabla} \times \vec{B}(\vec{r}, z) = 4\pi\vec{J}(\vec{r}, z)/c$. Upon setting $B = \vec{\nabla} \times \vec{A}_{3d}$ and using the Coulomb gauge, Ampere's law becomes

$$-\nabla^2 \vec{A}_{3d}(\vec{r}, z) + \frac{1}{\lambda_{\text{eff}}} \vec{A}_{2d}(\vec{r}) \delta(z) = \frac{s\phi_0}{2\pi\lambda_{\text{eff}}} \frac{\hat{z} \times \vec{r}}{r^2} \delta(z), \quad (2.78)$$

where $\nabla^2 = \nabla_{\perp}^2 + \partial^2/\partial z^2$ and we have inserted the phase gradient for a single vortex of charge s at the origin. We now pass to Fourier transformed vector potentials

$$\vec{A}_{3d}(\vec{q}_{\perp}, q_z) = \int d^2r \int dz e^{i\vec{q}_{\perp} \cdot \vec{r}} e^{iq_z z} \vec{A}_{3d}(\vec{r}, z) \quad (2.79)$$

and

$$\vec{A}_{2d}(\vec{q}_{\perp}) = \int d^2r e^{i\vec{q}_{\perp} \cdot \vec{r}} \vec{A}_{2d}(\vec{r}) \quad (2.80)$$

and find that (2.78) becomes

$$\vec{A}_{3d}(\vec{q}_{\perp}, q_z) + \frac{1}{\lambda_{\text{eff}}(q_z^2 + q_{\perp}^2)} \vec{A}_{2d}(\vec{q}_{\perp}) = \frac{is\phi_0}{\lambda_{\text{eff}}(q_z^2 + q_{\perp}^2)} \frac{\hat{z} \times \vec{q}_{\perp}}{q_{\perp}^2}. \quad (2.81)$$

The *2d* and *3d* vector potentials must agree on the plane $z = 0$, i.e., $\vec{A}_{3d}(\vec{r}, z = 0) = \vec{A}_{2d}(\vec{r})$, so that

$$\vec{A}_{2d}(q_{\perp}) = \int_{-\infty}^{\infty} \frac{dq_z}{2\pi} \vec{A}_{3d}(\vec{q}_{\perp}, q_z). \quad (2.82)$$

After integrating Eq. (2.81) over q_z and using this result we can solve for $\vec{A}_{2d}(\vec{q}_{\perp})$,

$$\vec{A}_{2d}(\vec{q}_\perp) = \frac{is\phi_0(\hat{z} \times \vec{q}_\perp)}{q_\perp^2(1 + 2\lambda_{\text{eff}}q_\perp)}. \quad (2.83)$$

Upon inserting Eq. (2.83) into the Fourier transform of Eq. (2.76) after setting $\vec{J}(\vec{r}, z) \equiv d\vec{J}_{2d}(\vec{r})\delta(z)$, we have

$$\vec{J}_{2d}(\vec{q}_\perp) = \frac{c}{2\pi} \frac{is\phi_0(\hat{z} \times \vec{q}_\perp)}{dq_\perp(1 + 2\lambda_{\text{eff}}q_\perp)} \quad (2.84)$$

and so the superconducting current in real space is

$$\vec{J}_{2d}(\vec{r}) = \frac{is\phi_0}{2\pi d} \int \frac{d^2q_\perp}{(2\pi)^2} \frac{e^{-i\vec{q}_\perp \cdot \vec{r}}}{(1 + 2\lambda_{\text{eff}}q_\perp)} \frac{\hat{z} \times \vec{q}_\perp}{q_\perp}. \quad (2.85)$$

The behavior of this screening current depends on the effective London penetration depth. For $r \ll \lambda_{\text{eff}}$, we find

$$\vec{J}_{2d}(\vec{r}) = \frac{sc\phi_0}{8\pi^2 d\lambda_{\text{eff}}r} \hat{\theta} \quad (2.86)$$

which agrees with the $r \ll \lambda_0$ limit of Eq. (2.74) for our “naive” model. This unscreened $1/r$ falloff now continues, however, out to a much larger distance $\lambda_{\text{eff}} = (\lambda_0/d)\lambda_0 \gg \lambda_0$. For $r \gg \lambda_{\text{eff}}$, the limiting behavior of (2.85) is

$$\vec{J}_{2d}(\vec{r}) = \frac{sc\phi_0}{4\pi^2 dr^2} \hat{\theta}. \quad (2.87)$$

The exponential screening of vortex currents in the “naive” model is thus replaced by a $1/r^2$ power-law falloff.

Similar results hold for the interactions between vortex pairs [30]. Vortices interact logarithmically, as into neutral superfluids for $r \ll \lambda_{\text{eff}}$, but exhibit a weaker $1/r$ potential for $r \gg \lambda_{\text{eff}}$. Since λ_{eff} can be of order fractions of a centimeter for film thicknesses $d = 10 - 100 \text{ \AA}$, the Kosterlitz-Thouless theory becomes directly applicable on essentially all length scales for sufficiently thin films [25]. The relatively weak screening compared to bulk systems arises because currents are confined to a thin plane instead of forming rings along the entire z axis.

III. DEFECTS IN MEMBRANES AND MONOLAYERS

Two-dimensional crystals have much in common with two-dimensional superfluids. There are many important experimental examples, including rare gases adsorbed onto periodic substrates like graphite, Langmuir-Blodgett films of amphiphilic molecules at air-water interfaces, freely suspended liquid crystal films, electron layers trapped at the surface of liquid

helium, and assemblies of colloidal particles confined between two glass plates [8,31]. Crystals consisting of a few atomic or molecular layers display algebraic decay of a translational order parameter, similar to Eq. (2.19), and the crystal elastic constants play a role similar to that of the superfluid density [8]. As emphasized by Kosterlitz and Thouless [1] and by Berezinski [2], dislocations in such crystals are point defects with a logarithmically diverging energy as a function of system size, and one might expect them to melt via a dislocation unbinding mechanism.

When the detailed dislocation unbinding theory was worked out [32,33], there was a surprise. Melting via dislocations leads not to an isotropic liquid, as proposed originally [1,2], but produces instead a new hexatic phase of matter, with residual bond orientational order [32]. The long-range bond orientational order in two-dimensional crystals at low temperatures is converted into algebraically decaying correlations in a hexatic fluid by a gas of unbound dislocations. Each dislocation, moreover, contains an embryonic pair of orientational defects called disclinations in its core. These disclinations separate and interact logarithmically in the hexatic phase, and themselves unbind via a second phase transition at sufficiently high temperatures. The latent heat associated with the usual first-order melting point can thus be spread out over an entire intermediate phase, separated from the low-temperature crystal and high-temperature liquid by two continuous phase transitions.

We call the experimental systems mentioned above “monolayers,” to emphasize that they are constrained to be approximately flat. In all cases, there are nearby substrates, walls or interfaces which force the degrees of freedom to “layer,” i.e., to lie a plane. Excitations out of the plane are strongly disfavored by, for example, a surface tension. There is, however, another important class of two-dimensional materials called “membranes” [34]. Membranes are two-dimensional associations of molecules different from the three-dimensional fluid medium in which they are embedded. Examples include lipid bilayers in water [34] or spectrin protein skeletons extracted from red blood cells [35]. Because membranes are not confined to an interface between two different phases, the surface tension vanishes and they exhibit wild fluctuations out the plane while retaining a local two-dimensional topology.

In this section, we review the physics of defects such as dislocations, disclinations, grain boundaries, vacancies and interstitials in membranes and monolayers. We discuss crystalline monolayers first, and then show how defect buckling screens defect energies in membranes [36–38]. The buckling transition of disclinations in hexatic membranes [39] is also described. We point out a fundamental asymmetry in the populations of positive and negative disclinations in liquid membranes with free boundary conditions or with fluctuating topologies. For a discussion of the spin-glass-like statistical mechanics of *polymerized* membranes with

quenched random distributions of defects such as impurity atoms, grain boundaries, see Refs. [40–42].

A. Landau Theory and Elasticity of Tethered Membranes

Consider first the statistical mechanics of two-dimensional assemblies of atoms and molecules *without* defects. To exclude defects, we assume a perfect triangular lattice of monomers embedded in three dimensions and *tethered* together via an unbreakable network of covalent bonds. Such “tethered surfaces” [43,44] exhibit interesting fluctuations and phase transitions even in the absence of defects. Once in the low temperature, broken symmetry phase of the relevant Landau theory, defects can be introduced for both monolayers and membranes.

Consider first the high temperature, crumpled phase of a tethered surface, similar to the crumpled state of a linear polymer chain. We describe the membrane by a function $\vec{r}(x_1, x_2)$, where \vec{r} is a three-dimensional vector specifying the position of the monomers as a function of two internal coordinates x_1 and x_2 fixed to the monomers. It turns out that the crumpled membrane can undergo a spontaneously symmetry-breaking into a flat phase below a crumpling temperature T_c [36]. The order parameters for this transition are the surface tangents $\{\vec{t}_\alpha = d\vec{r}/dx_\alpha, \alpha = 1, 2\}$ and the Landau free energy describing the transition is [45],

$$F[\vec{r}(x_1, x_2)] = \int d^2x \left[\frac{1}{2} \kappa (\partial_\alpha^2 \vec{r})^2 + \frac{1}{2} a (\partial_\alpha \vec{r})^2 + b (\partial_\alpha \vec{r} \cdot \partial_\beta \vec{r})^2 + c (\vec{\partial}_\gamma \vec{r} \cdot \partial_\gamma \vec{r})^2 + \dots \right] \quad (3.1)$$

Within this expansion in the tangents, the probability of a surface configuration $\vec{r}(x_1, x_2)$ is proportional to $\exp\{-F[\vec{r}(x_1, x_2)]/T\}$. Note that F is invariant under translations and rotations both within the embedding space and in the internal coordinates, as it should be. Self-avoidance between monomers at very different values of $\vec{x} = (x_1, x_2)$, but close together in the embedding space is neglected, although it is not hard to incorporate this into the model [45]. We assume that a changes sign at the mean field crumpling transition, $a = a'(T - T_c)$, just as in the more conventional Landau theories for superfluids discussed in Sec. II.

We discuss here only the low-temperature flat phase. When $a < 0$, F is minimized by

$$\begin{aligned} \vec{r}_0 &= \langle \vec{r}(x_1, x_2) \rangle \\ &= m[x_1 \vec{e}_1 + x_2 \vec{e}_2], \end{aligned} \quad (3.2)$$

where \vec{e}_1 and \vec{e}_2 are an arbitrary orthogonal pair of unit vectors in the three-dimensional embedding space and

$$m = \frac{1}{2} \sqrt{\frac{-a}{b+2c}}. \quad (3.3)$$

Note that $\langle \vec{t}_\alpha \rangle = \langle d\vec{r}/dx_\alpha \rangle = m\vec{e}_\alpha$, so that m is the ‘‘amplitude’’ of the tangent order parameters. The average of the surface tangents vanishes in the high-temperature phase, because the surface is highly crumpled. Additional physical insight is provided if we rewrite the free energy as

$$F = \text{const.} + \int d^2x \left\{ \frac{1}{2} \kappa (\partial_\alpha^2 \vec{r})^2 + \mu \left[\frac{\partial \vec{r}}{\partial x_\alpha} \cdot \frac{\partial \vec{r}}{\partial x_\beta} - m^2 \delta_{\alpha\beta} \right]^2 + \lambda \left[\frac{\partial \vec{r}}{\partial x_\gamma} \cdot \frac{\partial \vec{r}}{\partial x_\gamma} - 2m^2 \right]^2 \right\} \quad (3.4)$$

where

$$\mu = 4bm^4 \quad (3.5a)$$

and

$$\lambda = 8cm^4. \quad (3.5b)$$

This free energy is a sum of a bending energy, controlled by κ , and stretching contributions governed by elastic moduli μ and λ . The stretching terms provide an energetic penalty whenever the induced metric in the embedding space,

$$g_{\alpha\beta}(x_1, x_2) = \frac{\partial \vec{r}}{\partial x_\alpha} \cdot \frac{\partial \vec{r}}{\partial x_\beta}, \quad (3.6)$$

deviates from a flat background value

$$g_{\alpha\beta}^0 = m^2 \delta_{\alpha\beta}. \quad (3.7)$$

The low energy Goldstone modes associated with the flat phase are phonons. To study these excitations, we proceed as in the ‘‘phase only’’ approximation for superfluids [46] and set

$$\vec{r}(x^1, x^2) \approx m(x_1 + u_1)\vec{e}_1 + m(x_2 + u_2)\vec{e}_2 + f\vec{e}_3, \quad (3.8)$$

where $\vec{u}(x_1, x_2)$ is an in-plane phonon field and $f(x_1, x_2)$ is an out-of-plane displacement along $\vec{e}_3 = \text{vece}_1 \times \vec{e}_2$. With the neglect of an additive constant, the free energy (3.3) becomes

$$\begin{aligned}
F = \int d^2x & \left\{ \frac{\mu}{4} [\partial_\alpha u_\beta + \partial_\beta u_\alpha + (\partial_\alpha f)(\partial_\beta f)]^2 \right. \\
& \left. + \frac{\lambda}{2} [\partial_\gamma u_\gamma + \frac{1}{2} (\partial_\gamma f)^2]^2 + \frac{\kappa}{2} \int d^2x (\nabla^2 f)^2 \right\}. \tag{3.9}
\end{aligned}$$

This expression is identical to the energy of a bent elastic plate, where κ is bending rigidity, μ is a shear modulus, and $\mu + \lambda$ is the bulk modulus [47]. One often finds the stretching energy contributions written in terms of the nonlinear strain matrix $u_{\alpha\beta}(x_1, x_2)$

$$u_{\alpha\beta} = \frac{1}{2}(\partial_\alpha u_\beta + \partial_\beta u_\alpha) + \frac{1}{2}(\partial_\alpha f)(\partial_\beta f). \tag{3.10}$$

We have neglected terms nonlinear in \vec{u} , which are less important than the nonlinear terms in f which we have kept. It can be shown that the nonlinear terms in f cause the renormalized bending rigidity to *diverge* at long wavelengths, leading to the remarkable conclusion that the low-temperature flat phase represents a genuine broken continuous symmetry with true long-range order [34,36]. Broken continuous symmetries two-dimensional systems at finite temperatures are usually impossible, and are replaced instead by exponential decay of correlations or by algebraically decaying order such as that found for superfluid helium films in Eq. (2.19).

Note the similarity between Eq. (3.9) the free energy Eq. (2.59) which arose in our “naive” theory of superconducting films. The phase gradient $\vec{\nabla}\theta$ is replaced by the linearized strain matrix $\frac{1}{2}(\partial_\alpha u_\beta + \partial_\beta u_\alpha)$. The superfluid density is replaced by the elastic constants μ and λ . The role of the “vector potential” is played by gradients of f , and the bending rigidity contribution replaces the field energy term $\frac{1}{8\pi}|\vec{\nabla} \times \vec{A}|^2$ for superconductors. Because “vector potential” contribution to Eq. (3.10) is nonlinear, the two theories are certainly not identical. Nevertheless, we shall find striking similarities when we relax the constraint of perfect sixfold coordination and allow for defects: If we first set $f = 0$, then Eq. (3.9) can be used to calculate defect energies in planar “monolayers”—see below. Defects in monolayers are like the vortex singularities discussed earlier for neutral superfluids. When $f \neq 0$, however, the theory applies to the low-temperature phase of “membranes.” As we shall see, these defects are then screened by nonzero gradients of f , similar to the screening of vortices by the vector potential in superconductors. The corresponding reduction in energy for membranes is accompanied by defect buckling out of the plane defined by $f = 0$.

B. Defects in Monolayers

Fig. 7 shows a typical particle configuration for a thermally excited monolayer in its crystalline phase. Most particles, indicated by circles, have six nearest neighbors, as determined by the Dirichlet or Wigner-Seitz construction: The nearest neighbor coordination number of a particle is the number of edges of the minimal polygon formed by the bisectors of the lines connecting it to its near neighbors. The 5- and 7-fold coordinated particles (indicated by diamonds and asterisks, respectively) are orientational disclination defects in the otherwise 6-fold coordinated triangular lattice. An elementary application of Euler's theorem shows that the average coordination number with periodic boundary conditions must be exactly six [48], so the numbers of 5's and 7's must be equal. A high-temperature liquid can be viewed as a dense plasma of disclinations. The “plus” and “minus” disclinations (5's and 7's) in a liquid annihilate and pair up with decreasing temperature to form a crystal.

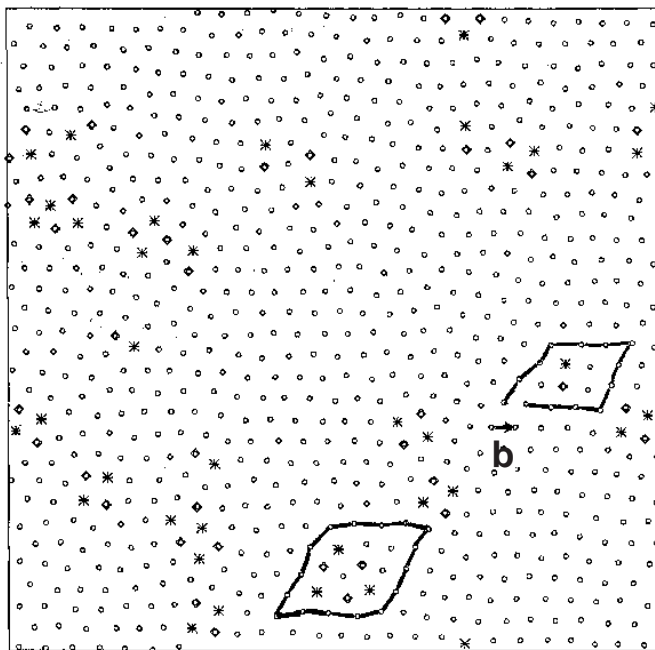


FIG. 7. Snapshot of a particle configurations in a computer simulation of a “monolayer.” Six-fold coordinated particles are shown as circles. Five-fold and seven-fold disclination defects are shown as diamonds and asterisks, respectively. Heavy contours surround a dislocation and an interstitial. From a simulation of classical electrons interacting with a repulsive $1/r$ potential by Rudolph Morf.

Disclination pairing is very evident in Fig. 7. An isolated disclination pair is, in fact, a dislocation defect. As illustrated in the figure, dislocations are characterized by the amount a path which would close on a perfect lattice fails to close. This mismatch, or “Burgers vector,” is a lattice vector of the underlying triangular crystal. It acts like a discrete vector “charge” attached to the dislocation, is independent of the exact contour chosen and points at right angles to a line connecting the 5 to the 7 in the dislocation core. More generally, such circuits determine the vector sum of all dislocation Burgers vectors contained inside. The Burgers circuit does in fact close for the other circuit shown in Fig. 7. The necklace of alternating 5’s and 7’s it contains can be viewed as three dislocations with radial Burgers pointing at 120 degree angles to each other. It represents a third type of defect, an interstitial. To see this, note that since the closed Burgers parallelogram is 4 lattice units on a side, it would enclose $3 \times 3 = 9$ particles if the lattice were perfect. In fact, there are 10 particles inside the contour, indicating the presence of an extra atom, or interstitial. The presence of a vacancy, the “antidefect” of the interstitial, could be detected by similar means.

To calculate the energies of the various monolayer defects discussed above, we use the continuum elastic free energy (3.9) with $f = 0$,

$$F = \frac{1}{2} \int d^2r [2\mu u_{ij}^2 + \lambda u_{kk}^2] \quad (3.11)$$

where

$$u_{ij} = \frac{1}{2} (\partial_i u_j + \partial_j u_i) . \quad (3.12)$$

In experimental monolayer systems, the constraint $f = 0$ might be imposed by a strong wall or substrate potential. For particles confined at an interface with a surface tension σ , we should add a term

$$\delta F = \frac{1}{2} \sigma \int d^2x (\vec{\nabla} f)^2 \quad (3.13)$$

to Eq. (3.9). Upon integrating out the f field in perturbation theory, and we recover a free energy of the form (3.11), with renormalized elastic constants μ and λ [49].

Dislocations, disclinations and other defects can be introduced into the theory in a way similar to the discussion of superfluid vortices in Sec. II. First, however, we determine the equations satisfied by free energy extrema away from defect cores. The variation of the monolayer free energy (3.11) with respect to \vec{u} leads to

$$\partial_i \sigma_{ij} = 0 , \quad (3.14)$$

where

$$\sigma_{ij} = 2\mu u_{ij} + \lambda u_{kk} \delta_{ij} \quad (3.15)$$

is the stress tensor. Equation (3.14) will be satisfied automatically if we introduce the Airy stress function χ via

$$\sigma_{ij}(\vec{r}) = \epsilon_{im} \epsilon_{jn} \partial_m \partial_n \chi(\vec{r}) . \quad (3.16)$$

The individual components of σ_{ij} are thus

$$\sigma_{xx} = \frac{\partial^2 \chi}{\partial y^2} , \quad \sigma_{yy} = \frac{\partial^2 \chi}{\partial x^2} , \quad \sigma_{xy} = -\frac{\partial^2 \chi}{\partial x \partial y} . \quad (3.17)$$

The function $\chi(\vec{r})$ is similar to the vector potential one uses to insure $\vec{\nabla} \cdot \vec{B} = 0$ in Maxwell's equations. If we are able to find χ , we know σ_{ij} , and hence the strain matrix by inverting Eq. (3.15),

$$\begin{aligned} u_{ij} &= \frac{1}{2\mu} \sigma_{ij} - \frac{\lambda}{4\mu(\mu + \lambda)} \sigma_{kk} \delta_{ij} \\ &= \frac{1}{2\mu} \epsilon_{im} \epsilon_{jn} \partial_m \partial_n \chi - \frac{\lambda \delta_{ij}}{4\mu(\mu + \lambda)} \nabla^2 \chi . \end{aligned} \quad (3.18)$$

So far, we have not used the important fact that u_{ij} is determined by gradients of a displacement field via Eq. (3.12). The corresponding requirement on the superfluid velocity, as given by Eq. (2.14), is

$$\vec{\nabla} \times \vec{v}_s = 0 , \quad (3.19)$$

which must hold away from vortex cores. The analogous compatibility condition on u_{ij} follows from applying the operator $\epsilon_{ik} \epsilon_{j\ell} \partial_k \partial_\ell$ to both sides of Eq. (3.18). This operator vanishes when acting on $u_{ij}(\vec{r})$, provided various derivatives of the displacement field commute. Equation (3.18) then simplifies to give a biharmonic equation of $\chi(\vec{r})$,

$$\begin{aligned} \frac{1}{K_0} \nabla^4 \chi(\vec{r}) &= \frac{1}{2} \epsilon_{ij} \epsilon_{j\ell} \partial_k \partial_\ell (\partial_i u_j + \partial_j u_i) \\ &= 0 , \end{aligned} \quad (3.20a)$$

with

$$K_0 = \frac{4\mu(\mu + \lambda)}{2\mu + \lambda} . \quad (3.20b)$$

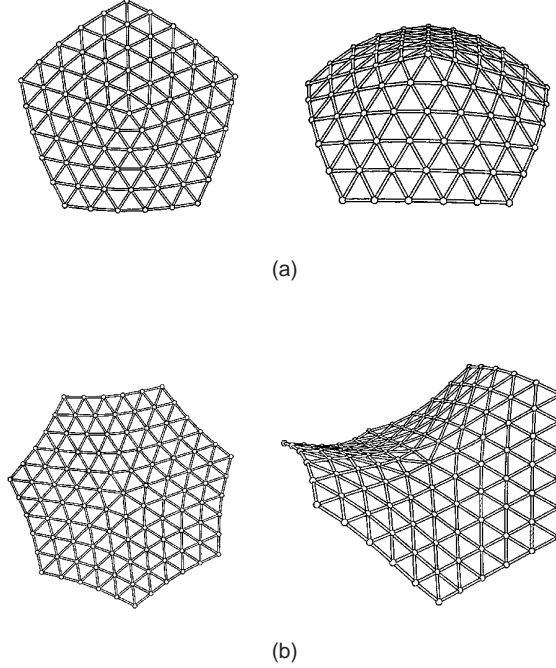


FIG. 8. Five- (a) and seven-fold (b) disclinations in monolayers (flat) and membranes (buckled). From Ref. [37].

Equation (3.20) must be satisfied “almost everywhere,” that is away from defect cores. Defects introduce source terms on the right-hand side, similar to the vortex density which appears in Eq. (2.34). As for superfluid vortices, defects represent points where derivatives fail to commute. Because the line integral of the differential bond angle field $\theta(\vec{r})$ around a disclination in a triangular lattice must be an integral multiple of $2\pi/6 = 60^\circ$,

$$\oint_{\mathcal{C}} d\theta(\vec{r}) = s \frac{2\pi}{6}, \quad (3.21)$$

we have

$$\epsilon_{ij} \partial_i \partial_j \theta(\vec{r}) = \frac{\pi}{3} \sum_{\alpha} s_{\alpha} \delta(\vec{r} - \vec{r}_{\alpha}) \quad (3.22)$$

for a collection of disclinations with “charges” $\{s_{\alpha} = \pm 1, \pm 2, \dots\}$ at positions $\{\vec{r}_{\alpha}\}$. Isolated 5- and 7-fold disclinations are shown in Fig. 8. The local bond angle $\theta(\vec{r})$ in a crystalline solid is given by the antisymmetric part of the strain tensor,

$$\begin{aligned} \theta(\vec{r}) &= \frac{1}{2} [\partial_x u_y(\vec{r}) - \partial_y u_x(\vec{r})] \\ &= \frac{1}{2} \epsilon_{k\ell} \partial_k u_{\ell}, \end{aligned} \quad (3.23)$$

so the noncommutativity of derivatives for disclinations takes the form,

$$\frac{1}{2}\epsilon_{ij}\epsilon_{kl}\partial_i\partial_j\partial_k u_\ell = \frac{\pi}{3}\sum_\alpha s_\alpha\delta(\vec{r}-\vec{r}_\alpha). \quad (3.24)$$

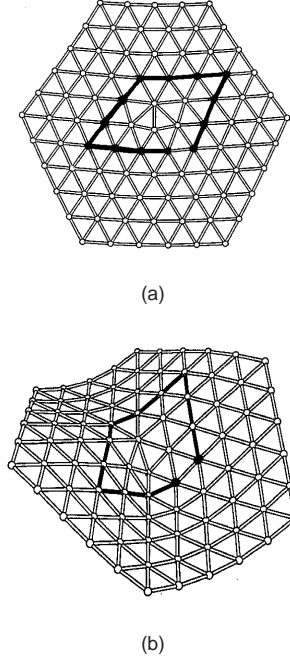


FIG. 9. Dislocation defect in a (a) monolayer (flat) and a (b) membrane (buckled). The burgers construction is shown in both cases. From Ref. [37].

We can treat dislocations by regarding them as tightly bound disclinations pairs, or alternatively by starting with the definition of the Burgers vector in the continuum limit

$$\begin{aligned} \oint_{\mathcal{C}} du_i &= \oint_{\mathcal{C}} \frac{\partial u_i}{\partial x_j} dx_j \\ &= b_i, \end{aligned} \quad (3.25)$$

where (see Fig. 9) the circuit \mathcal{C} encloses a single dislocation with Burgers vector \vec{b} . For a collection of Burgers “charges” $\{\vec{b}_\alpha\}$ at positions $\{\vec{r}_\alpha\}$, the differential statement of the noncommutivity embodied in constraints like (3.25) is

$$\epsilon_{kl}\partial_k\partial_\ell u_j = \sum_\alpha b_{\alpha i}\delta(\vec{r}-\vec{r}_\alpha). \quad (3.26)$$

Upon noting that the right-hand side of Eq. (3.20a) may be rewritten,

$$\frac{1}{2}\epsilon_{ik}\epsilon_{jl}\partial_k\partial_\ell(\partial_i u_j + \partial_j u_i) = \epsilon_{kl}\partial_k\partial_\ell\theta + \epsilon_{ip}\epsilon_{kl}\partial_p\partial_\ell\partial_k u_i, \quad (3.27)$$

we have, combining the above results for disclinations and dislocations,

$$\frac{1}{K_0}\nabla^4\chi(\vec{r}) = \sum_\alpha \epsilon_{ij}b_{\alpha i}\partial_j\delta(\vec{r}-\vec{r}_\alpha) + \frac{\pi}{3}\sum_\beta s_\beta\delta(\vec{r}-\vec{r}_\beta). \quad (3.28)$$

Vacancies and interstitials are special cases of a general class of “impurity defects” which includes as well substitutional atoms of the wrong size. If the defect sits in a lattice site of 3-fold or higher symmetry, its stress field is isotropic, and it can be characterized by the area deficit Ω_0 (positive or negative), it induces in an otherwise perfect lattice,

$$\begin{aligned}\Omega_0 &= \int (\vec{\nabla} \cdot \vec{u}) d^2r, \\ &= \oint_{\mathcal{C}} \hat{n} \cdot \vec{u}(\vec{r}) d\ell\end{aligned}\tag{3.29}$$

where \hat{n} is an outward unit normal to a contour \mathcal{C} surrounding an impurity at the origin. The biharmonic equation for $\chi(r)$ reads [47]

$$\nabla^4 \chi(\vec{r}) = -2\mu\Omega_0 \nabla^2 \delta(\vec{r}).\tag{3.30}$$

A similar equation can be derived for vacancies and interstitials by regarding them as three dislocations at the vertices of a small equilateral triangle with radial Burgers vectors pointing inward (vacancy) or outward (interstitial).

It is straightforward to rewrite the free energy (3.11) in terms of $\chi(r)$,

$$F = \frac{1}{2K_0} \int d^2r [\nabla^2 \chi(\vec{r})]^2.\tag{3.31}$$

Once $\chi(\vec{r})$ is known, we can thus calculate both the strain fields (from (3.18) and the defect energy. For an isolated disclination at the origin with angle defect s , we have [50]

$$\chi(\vec{r}) = \frac{K_0 s}{8\pi} r^2 [\ln(r/a) + \text{const.}]\tag{3.32}$$

and

$$F = \frac{K_0 s^2}{32\pi} R^2,\tag{3.33}$$

for a circular patch of crystal with radius R . Because disclination strains do not fall off at large distances, the free energy diverges *quadratically* with the size of the system. We have neglected a core energy contribution which is negligible as $R \rightarrow \infty$. For an isolated *dislocation* at the origin, one has

$$\chi(\vec{r}) = \frac{K_0}{4\pi} b_i \epsilon_{ij} r_j \ln(r/a)\tag{3.34}$$

and

$$F = \frac{K_0 b^2}{8\pi} \ln(R/a) + \text{const.}\tag{3.35}$$

The logarithmic divergence arises because the strains fall off like $1/r$, similar to the superfluid velocity in helium films.

The energy of isolated disclinations is prohibitively large in crystalline monolayers. This energy is reduced to a logarithmic divergence in the hexatic monolayers, however, because of screening by a gas of unbound dislocations [32]. The logarithmic energy of dislocations in two-dimensional crystals leads via the usual energy/entropy argument to an estimate of the dislocation unbinding temperature [1,2]. For a more detailed discussion of the statistical mechanics of defect mediated melting of monolayers, see Ref. [8].

For completeness, we note that the Airy stress function of an isolated impurity at the origin is

$$\chi(\vec{r}) = \frac{-\mu\Omega_0}{\pi} \ln(r/a) \quad (3.36)$$

corresponding to a displacement field

$$\vec{u}(\vec{r}) = \frac{\Omega_0 \vec{r}}{2\pi r^2}. \quad (3.37)$$

Because the strains now fall off as $1/r^2$, the elastic energy is finite and comparable to the core energy.

C. Defects in Crystalline Membranes

We now return to the full continuum elastic free energy Eq. (3.9) and determine how the defect energies are reduced in membranes, due to buckling into the third dimension. Variation of F with respect to f and \vec{u} leads to the von Karman equations [47]

$$\kappa \nabla^4 f = \frac{\partial^2 \chi}{\partial y^2} \frac{\partial^2 f}{\partial x^2} + \frac{\partial^2 \chi}{\partial x^2} \frac{\partial^2 f}{\partial y^2} - 2 \frac{\partial^2 \chi}{\partial x \partial y} \frac{\partial^2 f}{\partial x \partial y} \quad (3.38a)$$

$$\frac{1}{K_0} \nabla^4 \chi = - \frac{\partial^2 f}{\partial x^2} \frac{\partial^2 f}{\partial y^2} + \left(\frac{\partial^2 f}{\partial x \partial y} \right)^2 + S(\vec{r}). \quad (3.38b)$$

The Airy stress function is related to the stress as for monolayers, $\sigma_{ij}(\vec{r}) = \epsilon_{im}\epsilon_{jn}\partial_m\partial_n\chi(\vec{r})$, where we again have $\sigma_{ij} = 2\mu u_{ij} + \lambda u_{kk}\sigma_{ij}$. Now, however, u_{ij} is the nonlinear stress tensor,

$$\begin{aligned} u_{ij} &= \frac{1}{2}(\partial_i u_j + \partial_j u_i) + \frac{1}{2} \frac{\partial f}{\partial x_i} \frac{\partial f}{\partial x_j} + \frac{1}{2} \frac{\partial \vec{u}}{\partial x_i} \cdot \frac{\partial \vec{u}}{\partial x_j} \\ &\approx \frac{1}{2}(\partial_i u_j + \partial_j u_i) + \frac{1}{2} \frac{\partial f}{\partial x_i} \frac{\partial f}{\partial x_j}. \end{aligned} \quad (3.39)$$

In the first line of (3.39), we have included nonlinearities in the in-plane displacements \vec{u} . Although the nonlinearity in f is *always* important for membranes, the $\frac{1}{2} \frac{\partial \vec{u}}{\partial x_i} \cdot \frac{\partial \vec{u}}{\partial x_j}$ term can often be neglected. This terms *does* contribute significantly to disclination energies, however: In monolayers, for example, it leads to a small correction to the coefficient of the R^2 divergence in the disclination energy for monolayers [50]. In contrast to disclinations, the strain fields for dislocations and impurities fall off fast enough to justify neglecting the $\frac{1}{2} \frac{\partial \vec{u}}{\partial x_i} \cdot \frac{\partial \vec{u}}{\partial x_j}$ term in evaluating the far-field elastic energy. We have included a source term on the right-hand side of Eq. (3.38b) due to defects. For an isolated defect at the origin, one has

$$S(\vec{r}) = \begin{cases} \frac{\pi}{3} s \delta(\vec{r}), & \text{disclination,} \\ \epsilon_{ij} b_i \partial_j \delta(\vec{r}), & \text{dislocation,} \\ -\frac{2\mu+\lambda}{2(\mu+\lambda)} \Omega_0 \nabla^2 \delta(\vec{r}), & \text{impurity,} \end{cases} \quad (3.40)$$

just as in flat space. The additional contribution to the right-hand side of Eq. (3.38b) is the Gaussian curvature associated with the out-of-plane membrane displacements. This “curvature charge” can partially cancel the “topological charges” $S(\vec{r})$ of the defects when they buckle. Note that any solution with $f \neq 0$, implies another solution with $f \rightarrow -f$. When $f = 0$, we recover the elastic equations for monolayers.

1. Disclinations and Dislocations

Equations (3.38) are nonlinear and extremely difficult to solve analytically. Some progress is possible, however, in the inextensional limit $K_0 \rightarrow \infty$. All defect energies would be infinite in this case for monolayers. For membranes, however, defects can buckle so as to eliminate the elastic contributions to Eq. (3.9). The only remaining contribution is the bending energy. The required f field is determined by setting the right-hand side of Eq. (3.38b) to zero. The inextensional solutions of the von Karman equations representing a 5-fold disclination are

$$\chi(r) = -\kappa \ln(r/a_0), \quad f(r) = \pm \sqrt{\frac{1}{3}} r, \quad (3.41)$$

with energy

$$E_5 = \frac{1}{3} \pi \kappa \ln(R/a_0), \quad (3.42)$$

for a circular membrane with radius R . A 7-fold inextensional disclination can be represented in polar coordinates approximately by [36,37]

$$\chi(r) = 3\kappa \ln(r/a_0), \quad f(\vec{r}) = \pm \sqrt{\frac{2}{9}} r \sin 2\phi \quad (3.43)$$

which leads to an energy

$$E_7 = \pi\kappa \ln(R/a) . \quad (3.44)$$

The R^2 divergence of disclination energies in monolayers (with an *infinite* coefficient when $K_0 \rightarrow \infty$!) is thus screened considerably by buckling.

Precise numerical solutions of the von Karman equations for arbitrary κ and K_0 can be constructed by minimizing the energy of a triangulated tethered surface model [37]. The bending rigidity is represented by an interaction between neighboring unit normals to the triangular plaquettes and the in-plane elasticity by nearest neighbor harmonic springs adjusted to give the correct value of K_0 . This “dynamic triangulation” method is easier to implement than a direct numerical solution of the von Karman equations, and includes automatically all relevant nonlinearities. The numerical results for disclinations in the inextensional limit are similar to Eqs. (3.42) and (3.44), with slightly different coefficients [37]. It is still true that $F_5 < F_7$. Buckled disclinations obtained using this approach are shown in Fig. 8. Five-fold disclinations buckle into a cone, while the seven-fold disclination leads to a saddle surface. For disclinations and dislocations, the crucial physics lies in the existence of a buckling radius [36]: For small system radii R , these defects lie flat with no bending. Above a certain critical radius R_c , the defects trade elastic energy for bending energy and buckle out-of-the-plane. Numerical studies [37] show that disclination energies are screened down to a logarithmic divergence beyond the buckling radius, as suggested by results in the inextensional limit. Both disclinations and dislocations behave as if they were inextensional beyond the buckling radius.

Buckling is even more important for dislocations. Beyond the buckling radius R_b , the dislocation energy no longer increases logarithmically with R , and in fact appears to approach a finite constant [37]. A buckled dislocation is shown in Fig. 9. The entropic contribution to the dislocation free energy $F_d = E_d - S_d T$, however, still varies logarithmically with system size. The finiteness of the dislocation energy (or more precisely, *any* R dependence of the energy increasing more slowly than $\ln(R/a)$) then implies that untethered crystalline membranes must melt at *all* nonzero temperatures [36,37]. The areal density of dislocations in a hexatic membrane at temperature T is approximately

$$n_d \approx a_0^{-2} e^{-E_d/T} \quad (3.45)$$

where E_d is the (finite) dislocation energy, and a_0 is the lattice constant. Dislocations in membranes thus behave similarly to vortices in the “naive” model of superconducting films. Since buckled disclinations still have a logarithmically diverging energy, the hexatic fluid should be separated from a high-temperature isotropic liquid by a finite-temperature disclination unbinding transition (see below). Melting of membranes confined between two flat plates, which suppresses the buckling of dislocations and leads to a finite melting temperature $T_m(d)$, tending to zero as $d \rightarrow \infty$, has been studied by Morse and Lubensky [51].

Defects like dislocations and disclinations buckle into the third dimension when the cost in stretching energy to remain flat exceeds the bending energy required to buckle. More generally, buckling occurs whenever [38]

$$\frac{K_0 \ell^2}{\kappa} \geq \gamma \quad (3.46)$$

where ℓ is a characteristic length scale for the defect and γ is a dimensionless constant, typically of order 10^2 . In circular membranes of radius R , $\ell = \sqrt{Rb}$ for a dislocation with Burgers vector b , and $\gamma \approx 127$. For positive disclinations, we have $\ell = R$ and $\gamma \approx 160$, while for negative disclinations $\ell \approx R$ and $\gamma \approx 192$ [37]. Thus isolated dislocations and disclinations *always* buckle in sufficiently large crystalline membranes, irrespective of the values of the elastic constants.

Strictly speaking, these conclusions apply only at $T = 0$. In a finite temperature defect-free flat phase, thermal fluctuations cause the long wavelength wavevector dependent bending rigidity to diverge, $\kappa_R(q) \sim q^{-\eta_\kappa}$, while the renormalized elastic parameter $K_R(q)$ tends to zero $K_R(q) \sim q^{\eta_u}$ [36,52,53]. It is then appropriate to substitute $K_0/\kappa \rightarrow K_R/\kappa_R \sim 1/R^{\eta_\kappa + \eta_u}$ in Eq. (3.46). Using the values $\eta_\kappa = 0.82$ and $\eta_u = 0.36$ [53], we conclude that disclinations ($\ell \sim R$) will still buckle, while dislocations ($\ell \sim R^{1/2}$) become asymptotically flat as $R \rightarrow \infty$. Dislocations could still buckle on short scales, before these long wavelength thermal renormalizations of the elastic parameters set in. The dislocation energy will in any case tend to a finite constant for large R : Even if the dislocation remains asymptotically flat, we should now replace K_0 by $K_R(R) \sim 1/R^{\eta_u}$ in Eq. (3.35). Thus the conclusion that the hexatic phase is the stable low-temperature phase of membranes is unchanged.

2. Other Defects in Crystalline Membranes

Buckling is not inevitable even at $T = 0$ for finite energy defects such as vacancies, interstitials, or impurity atoms. The buckling criterion is again Eq. (3.46), where ℓ is

now related to the excess area induced by the defects, $\ell \approx \sqrt{\Omega_0}$ [38]. Buckling can be triggered in an *infinite* system simply by varying the ratio K_0/κ . Because of the finite length scale associated with these defects, it is the bare “local” values of K_0 and κ which should appear in (3.46). Since κ usually increases with increasing temperature, and K_0 usually decreases, buckling is most likely at low temperatures. The $f \rightarrow -f$ symmetry of the von Karman equations insures that buckled defects have at least two degenerate minima, representing displacements on opposite sides of the membrane. The ensemble of two-level systems generated by buckled finite energy defects will contribute to the specific heat and other equilibrium properties of membranes.

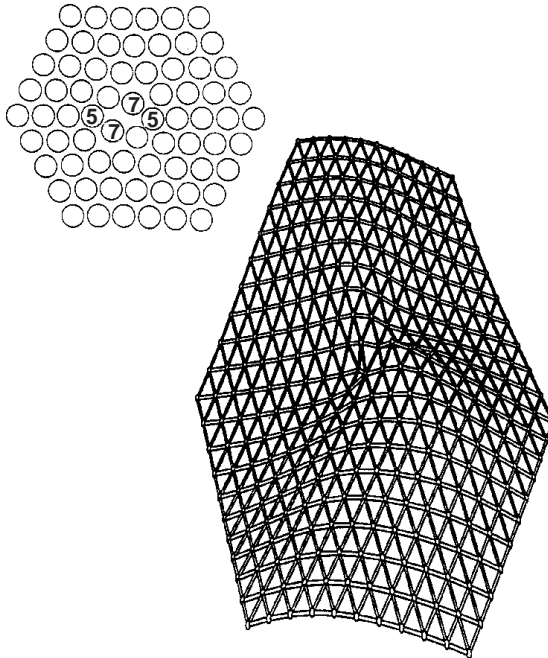


FIG. 10. Crushed vacancy defect in a flat monolayer and in a membrane. Note that the initial flat state, consists of two 5’s and two 7’s, and can be regarded as a tightly bound dislocation pair. From Ref. [38].

The buckling of a vacancy is illustrated in Fig. 10 [38]. Even in flat space, the vacancy does not have the high symmetry implied by the isotropic impurity source term in Eq. (3.40). For the harmonic spring nearest neighbor interaction potential used in Ref. [38], an initially six-fold symmetric vacancy is “crushed” into the lower symmetry object indicated in the figure. The crushed vacancy is equivalent to a tightly bound dislocation pair. Such vacancies buckle whenever $K_0 a_0^2/\kappa \gtrsim 26$ [38]. Figure 10b shows a buckled vacancy for $K_0 a_0^2/\kappa = 92$. Note that the 5-fold disclinations have buckled on opposite sides of the membrane.

It is also interesting to consider buckling of grain boundaries [38]. Three-dimensional crystals often consist of randomly oriented grains separated by defect walls. Similar polycrystalline order may appear in partially polymerized membrane vesicles [38,42,54]. In two dimensions, low-angle grain boundaries can be modeled by a row of dislocations, with average Burgers vector perpendicular to the boundary [55]. Consider first a grain boundary in a monolayer. Since all dislocations have the same sign, one might think that the elastic energy would be enormous. However, cancellations in the long-range part of the strain field insures a finite elastic energy per unit length [55]. Let θ be the tilt angle relating the mismatched crystallites on either side of the grain. A $\theta = 21.8^\circ$ grain boundary is shown in Fig. 11a. The spacing h between dislocations (associated with the large dots in Fig. 11a) is given by Frank's law [55], $h = \frac{1}{2}b \sin \frac{\theta}{2}$. On length scales large compared to h , the composite stress field of all the dislocations dies off exponentially, provided the Burgers vectors are strictly perpendicular to the boundary; on shorter scales, however, the behavior of the grain boundary should be dominated by the individual dislocations.

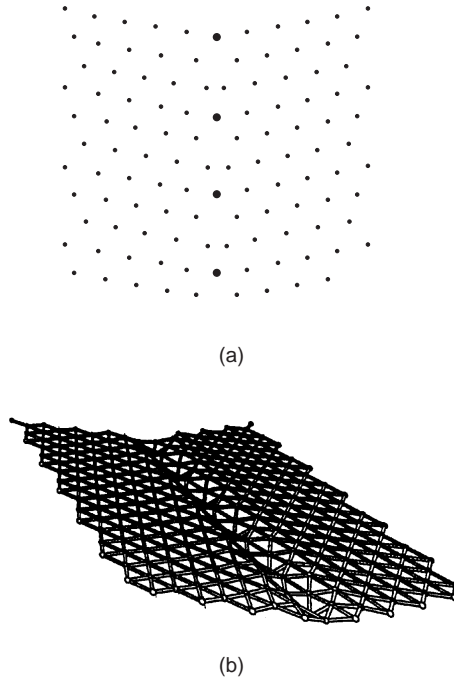


FIG. 11. Flat (a) and buckled (b) 21.8° grain boundaries. The two grains meet along the row of heavy dots. From Ref. [38].

Consider now a grain boundary inserted into a *membrane*. We have seen that isolated dislocations buckle whenever $R > R_b \approx 127\kappa/K_0b$. One might expect a similar buckling in grain boundaries whenever $h > R_b$. Numerical studies [38] show that Eq. (3.46) is again satisfied, with $\ell = \sqrt{bh}$ and $\gamma \approx 120$, consistent with this guess. A buckled 21.8° grain

boundary is shown in Fig. 11b for $K_0bh/\kappa = 300$. Note that the membrane remains *flat* far from the boundary.

D. Defects in Hexatic and Liquid Membranes

As discussed above, a finite concentration of unbound dislocations is present in membranes at any nonzero temperature. Provided disclinations remain bound together, the resulting phase is a hexatic, similar to the hexatic liquid which arises in the theory of two-dimensional melting of monolayers [32]. Hexatic fluids are characterized by extended correlations in the complex order parameter $\psi_6(\vec{r}) = \exp[6i\theta(\vec{r})]$, where $\theta(\vec{r})$ is the angle a bond between neighboring particles centered at \vec{r} makes with respect to a local reference axis. Because this reference axis changes when parallel transported on a curved surface, there is an important coupling between the bond angle field $\theta(\vec{r})$ and the geometry of membrane. This coupling stiffens hexatic membranes relative to their isotropic liquid membrane counterparts, although they still fluctuate more wildly than a crystalline tethered surface.

The continuum elastic-free energy for hexatic membranes was derived in Ref. [36]:

$$F_H = \frac{1}{2}K_A \int d^2r \left[\partial_i \theta - \frac{1}{2} \epsilon_{jk} \partial_k ((\partial_i f)(\partial_j f)) \right]^2 + \frac{1}{2} \kappa \int d^2r (\nabla^2 f)^2 \quad (3.47)$$

where K_A is the hexatic stiffness constant controlling fluctuations in $\theta(\vec{r})$. Note the similarity between F_H and the crystalline membrane energy Eq. (3.9). Both free energies contain a bending rigidity, and the out-of-plane displacements act like a “vector potential” coupled to the low energy Goldstone modes associated with the relevant broken symmetries. Hexatic membranes have many fascinating properties, including a “crinkled” phase, and an interesting literature is developing around them [56–58]. Here we discuss the von Karman equations for hexatics and show that they predict a buckling transition for positive disclination defect at a critical value of the ratio κ/K_A [39,59, 60]. We argue that the energy for negative disclinations must be different, and point out that this asymmetry has important consequences for liquid membranes once disclinations proliferate.

The variation of F_H with respect to f and θ leads to

$$\kappa \nabla^4 f = K_A (\partial_i \partial_j f) \epsilon_{jk} \partial_k (\partial_i \theta - A_i) , \quad (3.48)$$

and

$$\partial_i (\partial_i \theta - A_i) = 0, \quad (3.49)$$

with

$$A_i = \frac{1}{2} \epsilon_{jk} \partial_k ((\partial_i f)(\partial_j f)) . \quad (3.50)$$

In analogy to Eq. (3.16), we introduce a hexatic stress function χ_H (the Cauchy conjugate function for the hexatic “current”) via

$$K_A(\partial_i \theta - A_i) \equiv \epsilon_{ij} \partial_j \chi_H , \quad (3.51)$$

so that Eq. (3.49) is satisfied automatically. Now apply the operator $\epsilon_{ik} \partial_k$ to Eq. (3.51) and use Eq. (3.22) to rewrite the derivatives of θ in terms of the disclination density $S(\vec{r})$. The resulting equation, when combined with Eq. (3.48), results in the “von Karman equations for hexatics,” [39]

$$\kappa \nabla^4 f = \frac{\partial^2 \chi_H}{\partial y^2} \frac{\partial^2 f}{\partial x^2} + \frac{\partial^2 \chi_H}{\partial x^2} \frac{\partial^2 f}{\partial y^2} - 2 \frac{\partial^2 \chi_H}{\partial x \partial y} \frac{\partial^2 f}{\partial x \partial y} \quad (3.52a)$$

$$-\frac{1}{K_A} \nabla^2 \chi_H = -\frac{\partial^2 f}{\partial x^2} \frac{\partial^2 f}{\partial y^2} + \left(\frac{\partial^2 f}{\partial x \partial y} \right)^2 + S(\vec{r}) . \quad (3.52b)$$

Note that these equations are identical to Eqs. (3.38) except that $K_0 \rightarrow K_A$ and $\nabla^4 \rightarrow -\nabla^2$ in Eq. (3.52b).

Suppose $S(\vec{r}) = (+\pi/3)\delta(\vec{r})$, representing a single positive disclination at the origin. We then look for functions $\chi_H(\vec{r})$ and $f(\vec{r})$ of the form

$$\chi_H(r) = -\kappa \ln(r/a_0), \quad f(r) = \pm \alpha r \quad (3.53)$$

where α allows for conical dislocation buckling and remains to be determined. It is easy to check that Eq. (3.52a) is obeyed for arbitrary α . All three terms in Eq. (3.52b) are now proportional to delta functions, and equating the coefficients determines α ,

$$\alpha^2 = \frac{1}{3} - \frac{2\kappa}{K_A} . \quad (3.54)$$

For $\kappa/K_A > 1/6$, there are no real solutions and the membrane remains flat. For $\kappa/K_A < 1/6$, however, the disclination buckles [39]. Using Eq. (3.47) we readily find that the energy of this hexatic disclination in a membrane of radius R is

$$E_5 = \begin{cases} \frac{1}{3} \pi \kappa (1 - 3\kappa/K_A) \ln(R/a_0), & \kappa/K_A < \frac{1}{6}, \\ \frac{\pi K_A}{36} \ln(R/a_0), & \kappa/K_A > \frac{1}{6}. \end{cases} \quad (3.55)$$

When $\kappa/K_A > 1/6$, we recover the elastic energy for disclinations in flat hexatic monolayers [32]. When $K_A \rightarrow \infty$, we recover the buckled disclination energy (3.42) for crystalline membranes in the inextensional limit.

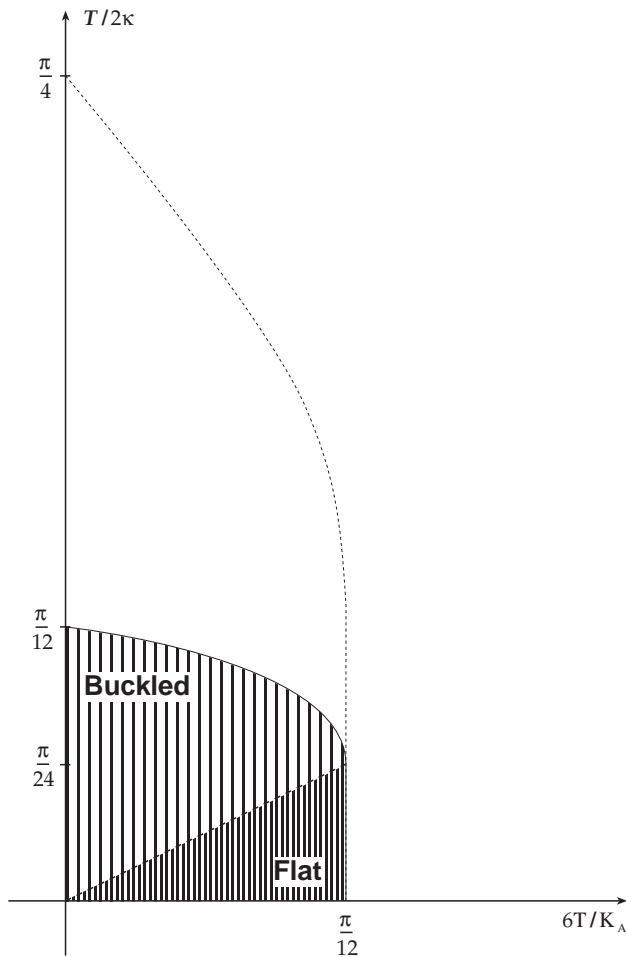


FIG. 12. Locus of entropic instabilities for a 5-fold disclination in a hexatic membrane (solid line). The shaded hexatic region is divided into regions where 5-fold disclinations buckle or remain flat, depending on the ratio K_A/κ . The dashed line is an estimate of where an isolated 7-fold disclination becomes unstable. The region above and to the right of the solid line is an isotropic fluid.

The total free energy of the 5-fold disclination including the positional entropy is

$$\begin{aligned}
 F_5 &= E_5 - ST \\
 &= E_5 - 2T \ln(R/a_0) .
 \end{aligned}
 \tag{3.56}$$

This free energy becomes negative above the solid line in Fig. 12. A curve of this kind was first presented by Gutter and Kardar [57], who used a more accurate theory to discuss the consequences of 5-fold disclination buckling. Their criteria for buckling and for disclination

proliferation are similar, but not identical to ours. Small errors are to be expected in our approach because the Gaussian curvature $G(r)$ in the Monge representation is actually

$$G(\vec{r}) = \frac{(\partial_x^2 f)(\partial_y^2 f) - (\partial_x \partial_y f)^2}{(1 + |\vec{\nabla} f|^2)^{1/2}}, \quad (3.57)$$

in contrast to the small $|\vec{\nabla} f|$ approximation which appears in Eq. (3.52b) [60]. A factor $(1 + |\vec{\nabla} f|^2)^{1/2}$ should also be included in the measure [60]. Nevertheless, the essential predictions of the two approaches are identical: the hexatic becomes unstable to an entropically driven proliferation of 5-fold disclinations whenever κ/T or K_A/T become sufficiently small.

What about *negative* disclinations? When $K_A \rightarrow \infty$ the similar approximations lead a result identical to the inextensional crystalline 7-fold defect described by Eq. (3.44). Although the energies of *both* 5- and 7-fold defects diverge logarithmically, the coefficient for negative disclinations is *larger*. This asymmetry persists (but is reduced slightly) in more accurate numerical computations [37]. When $\kappa \rightarrow \infty$, we approach the monolayer limit, and the 5- and 7-fold disclination energies will diverge logarithmically with *equal* coefficients. It seems plausible that the energy of a 7-fold disclination diverges logarithmically with system size for *arbitrary* values of κ/K_A , just as for the 5-fold disclinations. With the two above limits in mind, it seems clear that the free energy $F_7 = E_7 - 2T \ln(R/a_0)$ for negative disclinations only becomes negative above the dashed curve in Fig. 12. The energy/entropy argument seems to predict that positive and negative disclinations will unbind at two distinct temperatures! This conclusion, however, is probably incorrect. Consider the region between the solid and dashed lines in Fig. 12. Since the 5-fold defects are energetically favorable, the positive-free energy cost of a 7-fold defect can be compensated by a number of nearby 5-fold disclinations: A “composite defect” consisting of, say, one 7 and three 5’s will have a negative total free energy. Thus both positive and negative disclinations will proliferate above the solid line. A more complete theory of the disclination transition would include interactions between 5’s and 7’s and might also require overall disclination “charge neutrality.” Progress in this direction has recently been made by Park and Lubensky [58], although an explicit disclination asymmetry has not yet been incorporated into the theory.

The fundamental asymmetry between positive and negative disclinations should persist when hexatics melt into isotropic liquid membranes. Let us denote the defect core energies by E_5 and E_7 and assume that all long-range elastic energies have been screened out. Assume further that there is *no* constraint of disclination charge neutrality. This would be the case in membranes with free edges, or for the experimentally relevant case of liquid bilayer surfaces which can change their genus freely. The areal densities of disclinations will then be different,

$$n_5 \approx a_0^{-2} e^{-E_5/T}, \quad n_7 \approx a_0^{-2} e^{-E_7/T} . \quad (3.58)$$

Which defect predominates in liquid membranes depends on microscopic details such as interaction potentials, etc. Close to a transition to a hexatic phase, however, the arguments given above suggest that 5-fold disclinations dominate.

Disclination asymmetry in liquid membranes parallels the behavior of vacancies and interstitials in conventional crystalline solids [28]. Although vacancies and interstitials are the antidefects of each other, they nevertheless have very different energies. Unless vacancies and interstitials are created from a perfect crystal with periodic boundary conditions, they will in general occur with different concentrations. Periodic boundary conditions create an artificial constraint which forces vacancies and interstitials to be created in pairs rather than diffusing in from the surface. The concentrations must also be equal if the defects are charged, as in ionic crystals [28]. The flatness of monolayers similarly constrains the *disclination* densities to be equal at all stages in the theory of two-dimensional melting [32]. In membranes artificially constrained to have the topology of a toroidal surface, the numbers of 5- and 7-fold disclinations are forced to be equal to Euler's theorem. A calculation similar that for point defects in ionic crystals then leads to

$$n_5 = n_7 \approx a_0^{-2} e^{-(E_5+E_7)/2T} . \quad (3.59)$$

The free energy of liquid membranes is often expressed in the Helfrich form [62],

$$F_L = \frac{1}{2} \kappa \int d^2r (\nabla^2 f)^2 + \kappa_G \int d^2r [(\partial_x^2 f)(\partial_y^2 f) - (\partial_x \partial_y f)^2] . \quad (3.60)$$

The first term is the usual bending rigidity. The remaining one is proportional to the integrated Gaussian curvature and its coefficient κ_G is often called the Gaussian rigidity. This second term is a perfect derivative, and integrates to a constant for surfaces of fixed genus [34]. The microscopic origins of κ_G are obscure. Its sign, however, clearly determined by the disclination asymmetry discussed above: An excess of 5-fold disclinations corresponds to $\kappa_G < 0$ and favors *positive* net Gaussian curvature. Membrane phases many spherical vesicles will predominate in this case. An excess of 7-fold disclinations means $\kappa_G > 0$, and a bias toward negative Gaussian curvatures. Complex “plumbers nightmare” lipid membrane phases [34] are then favored.

On a more formal level, it must be the case from Euler's theorem that the Gaussian curvature integrated over a membrane with free edges of area Ω gives the disclination asymmetry

$$\int d^2r \sqrt{g} G(\vec{r}) = \Omega(n_5 - n_7) , \quad (3.61)$$

where $\sqrt{g} = 1 + |\vec{\nabla} f|^2$ and $G(\vec{r})$ is given by Eq. (3.57). Equation (3.60) can thus be rewritten as

$$F_L = \frac{1}{2}\kappa \int d^2r (\nabla^2 f)^2 + \kappa_G(N_5 - N_7) \quad (3.62)$$

where N_5 and N_7 are the total numbers of 5- and 7-fold disclinations in the membrane. The Gaussian rigidity κ_G thus acts as a chemical potential which must be adjusted to give the correct asymmetry between the populations of 5's and 7's. In this sense, its effect is similar to that of a nonzero magnetic field in Eq. (2.56), which would lead to a net excess of positive or negative vortices in superconducting films. For a related perspective on the physics of metallic glasses, see Ref. [62].

It would be interesting to search for the disclination asymmetry discussed here in computer simulations of membranes. The most straightforward approach would be to study initially flat (i.e., large κ) liquid membranes with free edges, so that disclinations can enter and exit freely at the boundary. When the bending rigidity is reduced, a bias in the average Gaussian curvature should emerge as the membranes curl up into the third dimension. One could then vary the interparticle potentials to study what factors influence the sign of $E_7 - E_5$. Such an understanding might lead to controlled synthesis of membranes with a predetermined sign of κ .

ACKNOWLEDGMENTS

I am grateful for the advice of E. Gitter, M. Kardar, T.C. Lubensky and J.D. Reppy while preparing this review. This work was supported by the National Science Foundation, through Grant No. DMR-9417047, and in part through the Harvard Materials Research Science and Engineering Center via Grant DMR-9400396.

APPENDIX: SUPERFLUID DENSITY AND MOMENTUM CORRELATIONS

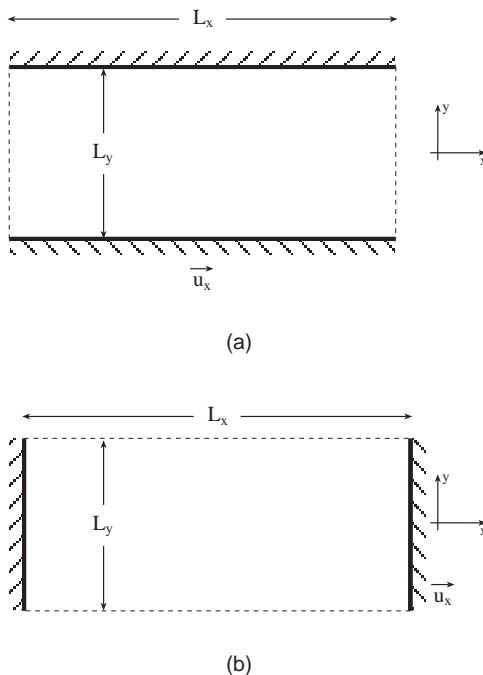


FIG. 13. Two experiments which lead to the superfluid density. In (a), there are periodic boundary conditions in the x direction, and impenetrable walls at $y = \pm L_y/2$. These boundary conditions are reversed in (b). In both cases, the walls and substrate move at velocity u_x in the x direction.

Consider a simplified version of the oscillating substrate experiment discussed in Sec. IIA. Imagine that the substrate is wrapped around to form a cylinder, coated uniformly with He^4 . We neglect substrate inhomogeneities, as is appropriate near the transition or if the films are sufficiently thick [63]. Now imagine that the substrate oscillations are around the cylinder axis, and slow enough so that the motion of the substrate is essentially a uniform translation with velocity \vec{u} . As illustrated in Fig. 13a, we choose a coordinate system such that the substrate moves along the x axis. The cylinder has height L_y along the y axis, and there are barriers at $y = \pm L_y/2$ which prevent the film from escaping in this direction. Its circumference is L_x . In two *or* three dimensions, the superfluid density measures the response of liquids to moving walls [20–22]. In Fig. 13a, the “walls” are provided by the substrate itself plus the barriers at the top and bottom of the cylinder. Instead of solving a complicated statistical mechanics problem with moving boundaries, it is easier to make a Galilean transformation to a coordinate system which moves at the velocity of the substrate, so that the boundaries are fixed. In the original laboratory frame of reference, the superfluid

fraction of the film will remain at rest. Hence, it appears to be moving with average velocity $-\vec{u}$ after the Galilean transformation.

If $\hat{\mathcal{H}}$ is the Hamiltonian in laboratory frame, averages after the Galilean transformation must be computed with respect to the Hamiltonian [64].

$$\hat{\mathcal{H}}' = \hat{\mathcal{H}} - \vec{u} \cdot \vec{P} + \frac{1}{2} M u^2, \quad (\text{A1})$$

where \vec{P} is the total momentum of the film and M is the total mass. Upon coarse graining the film, the free energy which appears in Eq. (2.10) is correspondingly replaced by

$$F' = F - \vec{u} \cdot \int \vec{g}(\vec{r}) d^2r + O(u^2), \quad (\text{A2})$$

where $\vec{g}(\vec{r})$ is given by Eq. (2.43). The relative weights of different configurations of $\psi(\vec{r})$ in the moving frame with stationary boundary conditions, given by $\exp[-F'/T]$, must be the same as those in the laboratory frame with moving boundary conditions. The average value of the momentum in the laboratory frame is thus given by

$$\langle g_i(\vec{r}) \rangle_{\vec{u}} = \frac{\int \mathcal{D}\psi(\vec{r}) g_i(\vec{r}) e^{-F'/T}}{\int \mathcal{D}\psi(\vec{r}) e^{-F'/T}}, \quad (\text{A3})$$

where $\vec{g} = (\hbar/2i)[\psi^*(\vec{r})\vec{\nabla}\psi(\vec{r}) - \psi(\vec{r})\vec{\nabla}\psi^*(\vec{r})]$ and the subscript on the average denotes a system with boundaries moving at velocity \vec{u} . To linear order in the wall velocity, we then have

$$\langle g_i(\vec{r}) \rangle_{\vec{u}} = \frac{1}{T} \int d^2r' \langle g_i(\vec{r}) g_j(\vec{r}') \rangle_{\vec{u}=0} u_j + O(u^2), \quad (\text{A4})$$

and we see that the momentum generated by moving walls in a helium film is determined by the momentum correlations for a system with the walls at rest. We now expand $\vec{g}(r)$ in Fourier variables,

$$\vec{g}(\vec{r}) = \frac{1}{\Omega_0} \sum_{\vec{q}} g(\vec{q}) e^{i\vec{q}\cdot\vec{r}}, \quad (\text{A5})$$

with

$$g(\vec{q}) = \int d^2r e^{-i\vec{q}\cdot\vec{r}} \vec{g}(\vec{r}), \quad (\text{A6})$$

and where Ω_0 is the system area. Equation (A4) can now be rewritten as

$$\langle g_i(\vec{r}) \rangle_{\vec{u}} = \frac{1}{T} \lim_{\vec{q} \rightarrow 0} C_{ij}(\vec{q}) u_j + O(u^2) \quad (\text{A7})$$

where

$$\begin{aligned}
C_{ij}(\vec{q}) &= \langle g_i(\vec{q})g_j(-\vec{q}) \rangle_{\vec{u}=0} \\
&\equiv A(q)\frac{q_iq_j}{q^2} + B(q)\left(\delta_{ij} - \frac{q_iq_j}{q^2}\right),
\end{aligned} \tag{A8}$$

and $A(q)$ and $B(q)$ are functions only of the *magnitude* of \vec{q} .

The coefficient of u_j Eq. (A7) involves a delicate limiting procedure whenever $A(q) \neq B(q)$ [20–22]. Consider first the situation outlined above, with the periodic boundary conditions in the x -direction appropriate to a smooth cylindrical substrate. For any finite cylinder circumference L_x , there are always Fourier components of the $\vec{g}(\vec{r})$ at $q_x = 0$, projected out by the x' integration in Eq. (A4). Along the y direction, however, the $q_y = 0$ mode only appears in the limit $L_y \rightarrow \infty$, because $\vec{g}(\vec{r})$ must vanish at the top and bottom of the cylinder. Thus, the correct order of limits for large sample sizes in this experiment is the limit $q_x \rightarrow 0$, followed by the limit $q_y \rightarrow 0$. The x component of the film momentum induced by the moving substrate is evidently

$$\begin{aligned}
\langle g_x(\vec{r}) \rangle_{\vec{u}} &= \frac{1}{T} \lim_{q_y \rightarrow 0} \lim_{q_x \rightarrow 0} C_{xx}(\vec{q})u_x \\
&= \frac{B(0)}{T} u_x.
\end{aligned} \tag{A9}$$

Since only the normal component of the film moves with the substrate, we identify $\rho_n(T)$ with the coefficient of u_x ,

$$\rho_n(T) = \frac{B(0)}{T}. \tag{A10}$$

Now consider a related, but fundamentally different experiment: We repeat the cylinder periodically along the y axis, but erect impenetrable barriers along the x axis at fixed positions $x = \pm L_x/2$. See Fig. 13b. The new barrier (equivalent to gouging a slit in the substrate parallel to the axis of the cylinder) prevents the film from circulating completely around the cylinder. The correct limiting procedure is now the limit $q_y \rightarrow 0$, reflecting the periodic boundary conditions along y , followed by the limit $q_x \rightarrow 0$, describing the new barriers in the limit $L_x \rightarrow \infty$,

$$\begin{aligned}
\langle g_x(\vec{r}) \rangle &= \frac{1}{T} \lim_{q_x \rightarrow 0} \lim_{q_y \rightarrow 0} C_{xx}(q)u_x \\
&= \frac{A(0)}{T} u_x.
\end{aligned} \tag{A11}$$

In this experiment, *all* of the film must clearly move at the substrate velocity since it is pushed around by the barrier. Now we identify ρ_{tot} , the total film density, with the coefficient of u_x , so that

$$\rho_{\text{tot}} = \frac{A(0)}{T} . \quad (\text{A12})$$

In a normal liquid, these two different limiting procedures would lead to identical results. In a superfluid, however, there is a nonzero superfluid density, defined by

$$\rho_s(T) = \rho_{\text{tot}} - \rho_n(T) . \quad (\text{A13})$$

The formula for the superfluid density is thus

$$\rho_s(T) = \frac{1}{T} \lim_{q \rightarrow 0} [A(q) - B(q)] . \quad (\text{A14})$$

REFERENCES

- [1] J. M. Kosterlitz and D. J. Thouless, J. Phys. **C5**, L124 (1972); J. Phys. **C6** 1181 (1973).
- [2] V.L. Berezinski, Zh. Eksp. Teor. Fiz. **59**, 907 (1970) [Sov. Phys. JETP **32**, 493 (1971); Zh. Eksp. Teor. Fiz. **61**, 1144 (1972) [Sov. Phys. JETP **34**, 610 (1972)].
- [3] P.G. deGennes in *Proc. of the Faraday Symposium on Liquid Crystals*, London, England (1971).
- [4] J. M. Kosterlitz, J. Phys. **C7**, 1046 (1974).
- [5] P. W. Anderson and G. Yuval, J. Phys. **C4**, 607 (1971).
- [6] J. M. Kosterlitz and D. J. Thouless, Prog. Low Temp. Phys. **78**, 371 (1978).
- [7] B.I. Halperin in *Physics of Low-Dimensional Systems*, edited by Y. Nagaoka and S. Hikami (Publication Office, Prog. in Theor. Physics, Kyoto, 1979).
- [8] D. R. Nelson in *Phase Transitions and Critical Phenomena*, edited by C. Domb and J.L. Lebowitz (Academic, New York, 1983), vol. 7.
- [9] V.A. Ambegaokar, B. I. Halperin, D. R. Nelson, and E. D. Siggia, Phys. Rev. **B21**, 1806 (1980).
- [10] B. I. Halperin and D.R. Nelson, J. Low. Temp. Phys. **36**, 599 (1979).
- [11] D. J. Bishop and J. Reppy, Phys. Rev. Lett. **40**, 1727 (1978); J.D. Reppy, in *Phase Transitions in Surface Films*, edited by J.G. Dash and J. Ruvalds (Plenum, New York 1980).
- [12] I. Rudnick, Phys. Rev. Lett. **40**, 1454 (1978).
- [13] See, e.g., A. N. Berker and D. R. Nelson, Phys. Rev. **B19**, 2488 (1979).
- [14] F.M. Gasparini, G. Agnolet and J.D. Reppy, Phys. Rev. **B29**, 138 (1984).
- [15] G. D. Mahan, *Many Particle Physics* (Plenum, New York, 1981), chapter 10.
- [16] O. Penrose and L. Onsager, Phys. Rev. **104**, 576 (1956).
- [17] I.M. Khalatnikov, *An Introduction to the Theory of Superfluidity* (W.A. Benjamin, New York, 1965).
- [18] F. Wegner, Zeit. für Physik **206**, 465 (1967); J.W. Kane and L.P. Kadanoff, Phys. Rev. **B155**, 80 (1967).

- [19] M. P. Kawatra and R. K. Pathria, *Phys. Rev.* **151**, 132 (1966).
- [20] P. C. Hohenberg and P. C. Martin, *Ann. Phys.* **34**, 291 (1965).
- [21] Gordon Baym, in *Mathematical Models in Solid State and Superfluid Theory*, edited by R. C. Clark and G. H. Berrick (Plenum, New York, 1968).
- [22] D. Forster, *Hydrodynamic Fluctuations, Broken Symmetry, and Correlation Functions* (Benjamin, Reading, MA, 1975).
- [23] D. R. Nelson and J. M. Kosterlitz, *Phys. Rev. Lett.* **39**, 1201 (1977).
- [24] J. Pearl, *Appl. Phys. Lett.* **5**, 65 (1964).
- [25] M. R. Beasley, J. E. Mooij, and T. P. Orlando, *Phys. Rev. Lett.* **42**, 1165 (1979).
- [26] M. Tinkham, *Introduction to Superconductivity* (McGraw-Hill, New York, 1975).
- [27] J. Toner and D.R. Nelson, *Phys. Rev.* **B23**, 316 (1981).
- [28] N. W. Ashcroft and N. D. Mermin, *Solid State Physics* (Holt Rinehart and Winston, Philadelphia, 1976), chapter 30.
- [29] For a detailed comparison of superfluidity in helium and in superconductors, see W.F. Vinen, in *Superconductivity*, edited by R.D. Parks (Marcel Dekker, New York, 1969), Vol. 2.
- [30] P.G. deGennes, *Superconductivity of Metals and Alloys* (Addison-Wesley, New York, 1989), Chapter 3.
- [31] See, e.g., the articles in *Bond Orientational Order in Condensed Matter Systems*, edited by K. Strandburg (Springer, New York, 1992).
- [32] B. I. Halperin and D. R. Nelson, *Phys. Rev. Lett.* **41**, 121, **E41**, 519 (1978); D. R. Nelson and B. I. Halperin, *Phys. Rev.* **B19**, 2457 (1979).
- [33] A. P. Young, *Phys. Rev.* **B19**, 1855 (1979).
- [34] See, e.g., the articles in D. R. Nelson, T. Piran, and S. Weinberg, *Statistical Mechanics of Membranes and Surfaces* (World Scientific, Singapore, 1989).
- [35] C. Schmidt *et al.*, *Science* **259**, 952 (1993).
- [36] D. R. Nelson and L. Peliti, *J. Phys. (Paris)* **48**, 1085 (1987).
- [37] S. Seung and D. R. Nelson, *Phys. Rev.* **A38**, 1005 (1988).

- [38] C. Carraro and D. R. Nelson, Phys. Rev. **E48**, 3082 (1993).
- [39] S. Seung, Ph.D. Thesis, Harvard University, 1990, unpublished.
- [40] L. Radzihovsky and D. R. Nelson, Phys. Rev. **A44**, 3525 (1991).
- [41] D. C. Morse and T. C. Lubensky, Phys. Rev. **A46**, 1751 (1992); and D. C. Morse, T. C. Lubensky, and G. S. Grest, Phys. Rev. **A45**, R2151 (1992).
- [42] D. R. Nelson and L. Radzihovsky, Phys. Rev. **A46**, 7474 (1992).
- [43] Y. Kantor, M. Kardar, and D. R. Nelson, Phys. Rev. **A35**, 3056 (1987).
- [44] Y. Kantor and D. R. Nelson, Phys. Rev. **A36**, 4020 (1987).
- [45] M. Paczuski, M. Kardar, and D. R. Nelson, Phys. Rev. Lett. **60**, 2638 (1988).
- [46] This similarity becomes clearer if one rewrites Eq. (2.12) as $\psi(\vec{r}) \approx \psi_0[1 + i\theta(\vec{r})]$ for small $\theta(r)$.
- [47] L. D. Landau and E. M. Lifshitz, *Theory of Elasticity* (Pergamon, New York, 1970).
- [48] See, e.g., L.K. Runnels in *Phase Transitions and Critical Phenomena*, Vol. 2, edited by C. Domb and M.S. Green (Academic, New York, 1972), J. P. McTague, D. Frenkel, and M. P. Allen, in *Ordering in Two Dimensions*, edited by S. Sinha (North-Holland, New York, 1980).
- [49] The calculations are similar to those for a *quenched f* field in S. Sachdev and D. R. Nelson, J. Phys. **C17**, 5473 (1984).
- [50] See, e.g., Ref. [37].
- [51] D. C. Morse and T. C. Lubensky, J. de Physique II, **3**, 531 (1993).
- [52] J. A. Aronovitz and T. C. Lubensky, Phys. Rev. Lett. **60**, 2634 (1988).
- [53] P. Le Doussal and L. Radzihovsky, Phys. Rev. Lett. **69**, 1209 (1992).
- [54] M. Mutz, D. Bensimon, and M. J. Brienne, Phys. Rev. Lett. **67**, 923 (1991).
- [55] J. P. Hirth and J. Lothe, *Theory of Dislocations* (Wiley, New York, 1992).
- [56] F. David, E. Guitter and L. Peliti, J. Phys. **49**, 2059 (1987).
- [57] E. Guitter and M. Kardar, Europhys. Lett. **13**, 441 (1990).
- [58] J.-M. Park and T.C. Lubensky, University of Pennsylvania, preprint.

- [59] E. Gutter, Ph.D. Thesis, Saclay 1990, and [57].
- [60] The *exact* energy for large R of an inextensional 5-fold crystalline disclination is $(11/30)\pi\kappa \ln(R/a_0)$ instead of Eq. (3.42) for similar reasons. See Ref. [39,8].
- [61] W. Helfrich, *Z. Naturforsch.* **28C**, 693 (1973).
- [62] D.R. Nelson and F. Spaepen in *Solid State Phys.*, vol. 42, edited by H. Ehrenreich and D. Turnbull (Harcourt Brance Jovanovich, New York, 1989).
- [63] Substrate disorder introduces quenched random fluctuations into the coefficient of $|\psi|^2$ in Eq. (2.11). Such randomness is known to be irrelevant if the specific heat exponent α is negative. The essential singularity in the specific heat at T_c may be interpreted as $\alpha = -\infty$.
- [64] E.M. Lifshitz and L.P. Pitaevskii, *Statistical Physics*, Part 2, (Pergamon, New York 1980) Sec. 23.